A copula-based model to describe the uncertainty of overtopping variables on mound breakwaters

Mares-Nasarre, Patricia; van Gent, Marcel R.A.; Morales-Nápoles, Oswaldo

DOI
10.1016/j.coastaleng.2024.104483

Publication date
2024

Document Version
Final published version

Published in
Coastal Engineering

Citation (APA)
Mares-Nasarre, P., van Gent, M. R. A., & Morales-Nápoles, O. (2024). A copula-based model to describe the uncertainty of overtopping variables on mound breakwaters. *Coastal Engineering*, *189*, Article 104483. https://doi.org/10.1016/j.coastaleng.2024.104483

Coastal Engineering 189 (2024) 104483

Contents lists available at ScienceDirect

Coastal Engineering

journal homepage: www.elsevier.com/locate/coastaleng

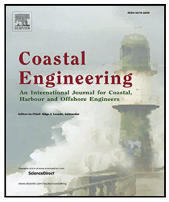

A copula-based model to describe the uncertainty of overtopping variables on mound breakwaters

Patricia Mares-Nasarre [a,*], Marcel R.A. van Gent [a,b], Oswaldo Morales-Nápoles [a]

[a] Faculty of Civil Engineering and Geosciences, Delft University of Technology, Delft, The Netherlands
[b] Deltares, Delft, The Netherlands

ARTICLE INFO

Keywords:
Overtopping
Overtopping layer thickness
Overtopping flow velocity
Overtopping volume
Uncertainty
Copula
Mound breakwater
Probability
Dependence

ABSTRACT

Rising sea levels caused by climate change are increasing the risk of overtopping on coastal structures. Moreover, there is a growing societal concern about the visual impact of these structures, which leads to the lowering of their crest freeboards. In previous studies, safety during overtopping events was assessed considering the overtopping layer thickness (h_c), the overtopping flow velocity (u_c) and the individual wave overtopping volume (V). Existing models in the literature to estimate h_c, u_c and V on mound breakwater crests are mainly deterministic, involve a chain of successive estimations leading to accumulated errors and/or do not account for the dependencies between h_c, u_c and V. This study proposes a model to describe the joint probability distribution of h_c, u_c and V based on bivariate copulas. Experimental data from small-scale 2D physical tests conducted on mound breakwaters with three armor layers (single-layer Cubipod®, and double-layer cubes and rocks) in depth-limited breaking wave conditions on two mild bottom slopes and dimensionless crest freeboards between 0.33 and 3.20 is used. Lognormal distribution functions are proposed for each variable and a multivariate dependence model is developed through a one-tree vine-copula. The parameters of this model are quantified directly using wave characteristics and the structure geometry minimizing the accumulated errors in the final predictions. The application of the model is illustrated by computing the probability of not fulfilling at least a tolerability limit for one of the studied variables (OR probability). The OR probability is computed both considering the dependence and assuming independence between the variables and a significant difference is obtained. It is concluded that by accounting for the multivariate dependence between the variables, it is possible to reduce the crest freeboard and, thus, achieve a more economic design within the required safety level.

1. Introduction

Sea level rise (IPCC, 2019) and stronger wave conditions (Camus et al., 2019) resulting from climate change have led to an increase of coastal hazards, such as the risk of salinization and flooding in low lying areas or the potential damage to the existing coastal structures. Moreover, since sustainable development was first defined by the Brundtland Commission (WCED, 1987), the awareness of society regarding the negative impacts of infrastructures has arisen and has sparked a demand for coastal structures with reduced visual and environmental impacts. These factors significantly influence the design of coastal structures; more extreme and uncertain wave overtopping events and reduced design dimensionless crest freeboards must be considered.

Thus, the current context of climate change has increased the uncertainty surrounding wave overtopping, which was already recognized as a highly uncertain phenomenon by Romano et al. (2015). Romano et al. (2015) studied the variability of the mean wave overtopping discharge (q, l/s/m) for different time series realizations from the same wave spectrum and concluded that q may vary up to one order of magnitude. Therefore, further non-deterministic tools are needed to improve the design of mound breakwaters facing extreme overtopping rates.

During the design phase, tolerable q is usually considered to determine the required crest elevation of coastal structures. However, overtopping hazard can be better described if the hydrodynamic variables of the individual wave overtopping events (namely, individual wave overtopping volumes, V (l), overtopping layer thickness on the crest, h_c (m), and overtopping flow velocity on the crest, u_c (m/s)) are included in the analysis (Franco et al., 1994). For instance, the maximum V (V_{max}) has been related to damage to coastal structures and hazard for vehicles and pedestrians (Geeraerts et al., 2007). h_c and

* Corresponding author.
E-mail addresses: p.maresnasarre@tudelft.nl (P. Mares-Nasarre), m.r.a.vangent@tudelft.nl (M.R.A. van Gent), o.moralesnapoles@tudelft.nl (O. Morales-Nápoles).

https://doi.org/10.1016/j.coastaleng.2024.104483
Received 13 September 2023; Received in revised form 5 February 2024; Accepted 5 February 2024
Available online 8 February 2024

u_c have also been related to the hydraulic stability of the breakwater crest and rear side (Argente et al., 2018) and the pedestrian safety on the breakwater crest (Bae et al., 2016).

In the last years, extensive literature has been developed to estimate h_c, u_c and V on mound breakwaters based on results of physical model tests (e.g., Mares-Nasarre et al., 2021; Koosheh et al., 2021). Regarding V, the 2-parameter Weibull distribution function has been extensively proposed to describe the univariate uncertainty of V (Franco et al., 1994; Besley, 1999; Bruce et al., 2009; Zanuttigh et al., 2013; Nørgaard et al., 2014; Molines et al., 2019). The maximum individual wave overtopping volume (V_{max}) was then estimated using the number of overtopping events (N_{ow}) which was predicted using q. This approach presents two main drawbacks: (1) the inclusion of a chain of estimations ($q - N_{ow} - V_{max}$) which lead to accumulated errors in the final predictions, and (2) the low reliability of the measurements of V_{max}, which is also function of the duration of the wave storm.

Regarding h_c and u_c on mound breakwaters, limited literature is available. Formulas to estimate h_c and u_c exceeded by 2% of the incoming waves ($h_{c,2\%}$ and $u_{c,2\%}$, respectively) were proposed in Mares-Nasarre et al. (2019, 2021). Also, the distribution function of events more extreme than $h_{c,2\%}$ and $u_{c,2\%}$ were analyzed. Exponential and Rayleigh distributions were recommended to describe the distribution functions of $h_c/h_{c,2\%}$ and $u_c/u_{c,2\%}$, respectively, where h_c and u_c are events extremer than 2%. It should be noted that the probabilities assigned to those observations of h_c and u_c were in terms of the number of incoming waves and not in terms of the commonly used exceedance probabilities (following van Gent, 2003; Schüttrumpf and van Gent, 2004). These methodologies have thus the pitfall of defining probabilities as function of the duration of the storm (number of waves) which hinders the comparison with probabilities obtained for V or wave characteristics. Moreover, it is required to estimate $h_{c,2\%}$ and $u_{c,2\%}$ to quantify the distribution of extreme values of h_c and u_c since they are defined in terms of $h_c/h_{c,2\%}$ and $u_c/u_{c,2\%}$, respectively, leading again to accumulated errors in the final estimations.

When designing the crest elevation of a mound breakwater using h_c, u_c and V, a given value of them (namely, $h_{c,2\%}$, $u_{c,2\%}$ and V_{max}) is compared to the tolerability limits and a binary result is obtained: the design satisfies or does not satisfy the limits. Consequently, a lot of information is lost regarding how likely it is to overpass those limits and, thus, what the safety level of the structure is. If the distribution functions proposed in the literature are used to determine the probabilities of overpassing those limits, the dependence between the variables is not considered. It is possible to determine the probability of not fulfilling one specific limit but if more than one tolerability limit is set (for instance to each of the three parameters h_c, u_c and V) the probability of not fulfilling at least one tolerability limit (OR probability) cannot be computed. This is, first, because probabilities for h_c and u_c are defined in terms of percentage of exceeded waves and probabilities for V are stated using the common axiomatic concept of probability. Thus, they cannot be combined. Second, if this difference is neglected, independence between the variables would need to be assumed. However, h_c, u_c and V are generated by the same drivers and, thus, a correlation exist between them. Therefore, a dependence model which describes the multivariate uncertainty of h_c, u_c and V all together is needed to better assess the crest elevation of mound breakwaters, as well as to provide further insight into their safety against overtopping.

In the Coastal Engineering field, copula-based models have been successfully used in the scientific literature to model the joint probability distribution of wave variables (e.g., Jaeger and Morales-Nápoles, 2017; Lucio et al., 2020) or to perform reliability assessments of structures or offshore operations (e.g., Leontaris et al., 2016; Torres-Alves and Morales-Nápoles, 2020). For instance, Antão and Guedes Soares (2014) and Jaeger and Morales-Nápoles (2017) focused on the probabilistic dependence between wave height and period to better model important asymmetries observed in their joint distribution by means of probabilistic models based on bivariate copulas. Masina et al. (2015), Corbella and Stretch (2013) and Sebastian et al. (2017) assessed coastal risk of flooding modeling the dependence between wave variables, storm surge and/or precipitation using copulas. Studies such as De Michele et al. (2007), Zhang et al. (2018), Lira-Loarca et al. (2020) or Leontaris et al. (2016) modeled wave storms using both bivariate and multivariate models based on copulas to assess and design coastal and offshore structures. However, to the authors' knowledge, copulas have not been used to model the response of coastal structures to wave loading.

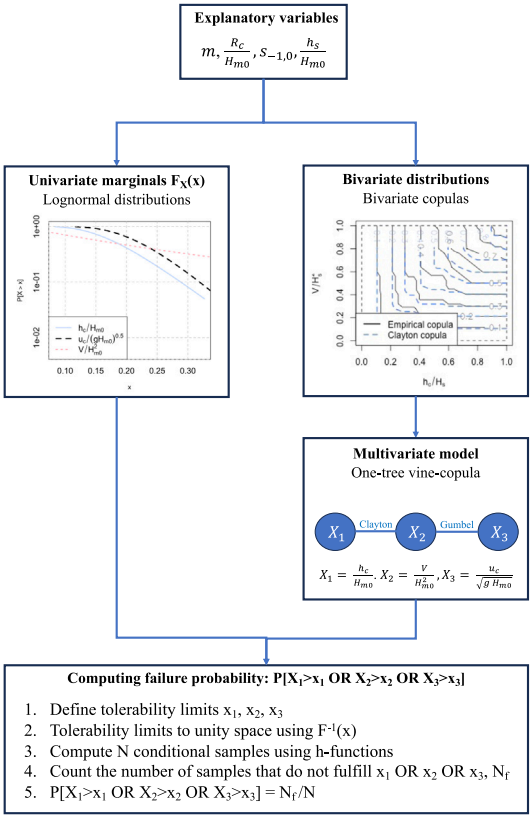

Fig. 1. Proposed methodology to compute the OR probability.

This study proposes a model to describe the joint probability distribution of h_c, u_c and V based on bivariate copulas. The contribution of this paper is three fold: (1) new distribution functions are proposed for each variable using the axiomatic probability concept, (2) a multivariate dependence model is developed, and (3) the parameters of both the marginals and dependence model are quantified directly using variables related to wave characteristics and the structure geometry minimizing the accumulated errors in the final predictions. Thus, this model allows the computation of the probability if more than one tolerability criterion is set. Conditional distributions and conditional probabilities can also be computed if the value of one or two variables is known. The paper is structured as follows. The experimental methodology of the physical model tests and data analysis of the measurements used to develop the proposed model is presented in Section 2. The concept of bivariate copula and the goodness of fit measures for these probabilistic models are introduced in Section 3. The selection and fitting of the new proposed distribution functions to describe the univariate uncertainty of h_c, u_c and V are described in Section 4. The selection and development of the copula-based model is described in Section 5. Recommendations of use together with an example of application of the proposed methodology are presented in Section 6 and illustrated in Fig. 1. Finally, conclusions are drawn in Section 7 and recommendations for future research are given.

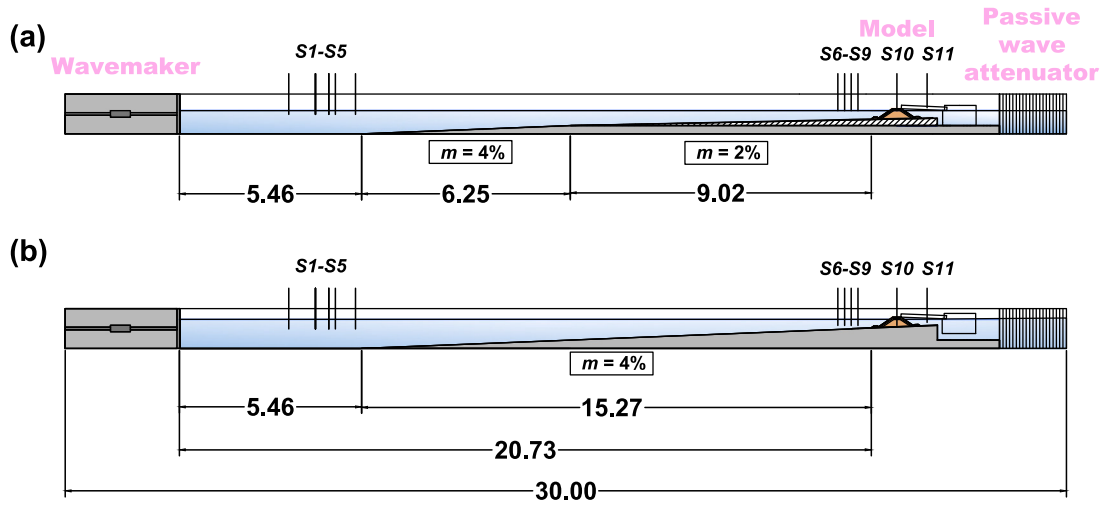

Fig. 2. Cross-section of the wave flume of LPC-UPV. Dimensions in m.

2. Experimental methodology

2.1. Experimental setup

2D physical tests were performed by Mares-Nasarre et al. (2021) in the wave flume (30 m × 1.2 m × 1.2 m) of the Laboratory of Ports and Coasts at Universitat Politècnica de València (LPC-UPV). Two bottom slope configurations were tested: (a) a 6.25 m-long $m = 4\%$ bottom slope and a 9.0 m-long $m = 2\%$ bottom slope, and (b) a continuous ramp of $m = 4\%$ all along the wave flume. Fig. 2 displays the longitudinal cross-sections tested in the wave flume and the locations of the wave gauges.

The LPC-UPV wave flume also presents a double floor to allow the water recirculation and prevent the accumulation of overtopped water behind the structure leading to a reduction of the water level at the seaward side. As shown in Fig. 2, wave gauge S11 was placed behind the model to detect this phenomenon; accumulation of water behind the structure was not significant during the tests. In addition, 10 more capacitive wave gauges were installed along the flume to measure the free surface. Wave gauges S1 to S5 were located close to the wave generator with distances following recommendations in Mansard and Funke (1980). These wave gauges were used to separate incident and reflected waves in the generation zone. Wave gauges S6 to S9 were placed in the model zone, where depth-limited wave breaking takes place. Note that the existing methods in the literature to separate incident and reflected waves are not reliable under these conditions, although de Ridder et al. (2023) showed that the incident significant wave heights can still be derived with rather good accuracy. S6, S7, S8 and S9 were installed at distances of $5h_s$, $4h_s$, $3h_s$ and $2h_s$ from the toe of the model, where h_s is the water depth at the toe of the structure. Wave gauge S10 was located in the middle of the breakwater crest to measure the overtopping layer thickness on the crest, h_c. All wave gauges measured at a frequency of 20 Hz.

Three different mound breakwater models were tested with armor slope H/V = 3/2 and rock toe berms: a single-layer Cubipod®-armored model (Cubipod-1L, nominal median diameter or equivalent cube size $D_n = 3.79$ cm), a double-layer randomly-placed cube-armored model (cube-2L, $D_n = 3.97$ cm) and a double-layer randomly-placed rock-armored model (rock-2L, $D_{n50} = 3.18$ cm). A cross-section of a tested model is depicted in Fig. 3. Tests performed on the bathymetry with $m = 2\%$ were conducted with a rock toe berm with nominal diameter or equivalent cube size $D_{n50} = 2.6$ cm, whereas those with $m = 4\%$ were carried on with a larger rock toe berm with $D_{n50} = 3.9$ cm to guarantee the toe berm hydraulic stability during the tests.

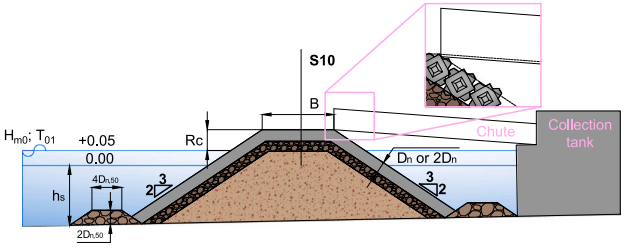

Fig. 3. Cross-section of the models tested in this study. Dimensions in m.

Random runs of 1000 irregular waves were generated following a JONSWAP spectrum ($\lambda = 3.3$). The AWACS wave absorption system was used during the tests to avoid multireflections in the flume; low-frequency oscillations were not significant during the tests. Two water depths at the toe (h_s) were tested for each model and bathymetry configuration. $h_s = 0.20$ m and 0.25 m were tested for all cases, but for those conducted with the cube-2L and $m = 2\%$ where $h_s = 0.25$ m and 0.30 m were tested. For each water depth and foreshore configuration, the spectral significant wave height ($H_{m0} = 4(m_0)^{0.5}$) and peak period (T_p) were generated such that the wave steepness ($s_{op} = H_{m0}/L_{op} = 2\pi H_{m0}/(gT_p^2)$, where L_{op} is the deep-water wave length) was kept approximately constant during the test series. For each $s_{op} = 0.02$ and 0.05, H_{m0} in the wave generation zone was increased in steps of 1 cm from no damage to initiation of damage of the armor model or wave breaking in the wave generation zone. The main experimental ranges of the experiments are shown in Table 1. Note that H_{m0} and spectral wave period ($T_{m-1,0} = m_{-1}/m_0$, where m_i is the ith spectral moment $m_i = \int_0^\infty S(f) f^i df$, being the wave spectrum $S(f)$) are provided using the incident waves near the toe of the structure.

2.2. Wave analysis

Waves were separated in the wave generation zone applying the LASA-V method (Figueres and Medina, 2005) on the measurements of wave gauges S1 to S5. This method is applicable to nonstationary and nonlinear irregular waves, but it is not valid for breaking waves, similarly to most methods in the literature. Therefore, the SwanOne propagation model (Verhagen et al., 2009) was used to estimate incident waves in the model zone, where wave breaking takes place. SwanOne model uses a JONSWAP spectrum ($\gamma = 3.3$) fitted with the incident wave conditions in the wave generation zone. Such spectrum is propagated along the flume and the wave height distribution

Table 1
Experimental ranges in the tests. Note that wave characteristics are given at the toe of the structure.

m	Armor	B (m)	#test	h_s (m)	R_c (m)	H_{m0} (m)	$T_{m-1,0}$ (s)
4%	Cubipod®-1L	0.24	28	0.20	0.12	0.06–0.15	0.93–2.05
			30	0.25	0.07	0.06–0.18	0.91–2.34
4%	cube-2L	0.27	30	0.20	0.16	0.05–0.16	0.95–2.10
			30	0.25	0.11	0.06–0.17	0.94–2.43
4%	rock-2L	0.26	19	0.20	0.15	0.05–0.14	0.92–2.04
			17	0.25	0.10	0.05–0.14	0.88–2.06
2%	Cubipod®-1L	0.24	30	0.20	0.12	0.06–0.14	0.91–2.21
			30	0.25	0.07	0.06–0.16	0.94–2.24
2%	cube-2L	0.27	30	0.25	0.11	0.05–0.16	0.95–2.25
			24	0.30	0.06	0.06–0.18	0.91–2.05
2%	rock-2L	0.26	15	0.20	0.15	0.06–0.12	0.90–1.86
			15	0.25	0.06	0.05–0.13	0.90–1.88

is described using the Composite Weibull distribution recommended by Battjes and Groenendijk (2000). Since SwanOne is prepared for prototype scale wave conditions (frequencies in the range 0.03 to 0.8 Hz), a scale 1/30 was used.

In order to validate this methodology, tests without structure were performed in Mares-Nasarre et al. (2021) using a passive wave absorption system at the end of the wave flume, similarly to Herrera and Medina (2015). The total measurements of the tests without a structure were compared to the simulations by SwanOne model both in the wave generation zone and in the model zone. The performance of SwanOne model was assessed using the coefficient of determination, R^2. $0 \leq R^2 \leq 1$ estimates the percentage of the variance explained by the model and is defined in Eq. (1).

$$R^2 = 1 - \frac{\frac{1}{N_{obs}} \sum_{i=1}^{N_{obs}} (o_i - e_i)^2}{\frac{1}{N_{obs}} \sum_{i=1}^{N_{obs}} (o_i - \bar{o})^2} \quad (1)$$

where N_{obs} is the number of observations, o_i and e_i are the observations and estimations, respectively, and $\bar{o}$ is the mean of the observations.

In line with previous studies (Mares-Nasarre et al., 2019, 2020b), satisfactory performance was obtained for H_{m0} ($R^2 \leq 0.94$), while poor performance was found for $T_{m-1,0}$ ($0.03 \leq R^2 \leq 0.89$). Similarly to Herrera and Medina (2015) or Mares-Nasarre et al. (2020b), wave characteristics estimated by SwanOne model were used for further analysis to simulate the design phase conditions, when the design wave conditions at the construction site need to be estimated. Note that the SwanOne model does not very accurately model the wave period since some essential physical processes are missing in this model. This often leads to an underestimate of the wave period. This bias in computed wave periods is taken into account by using SwanOne predictions to develop the model proposed in this study, as SwanOne is commonly use in practice.

2.3. Analysis of overtopping variables

A weighing system was installed in a collection tank behind the model to measure the overtopping discharges during each test. They were collected using a chute in the rear side line of the crest. This system provided a continuous record of accumulated overtopping volume and the individual wave overtopping volumes were identified following the method developed by Molines et al. (2019) based on the derivative of the overtopping record. Fig. 4 presents an example of the overtopping volume collected by the weighing system and the points identified as the beginning of an individual wave overtopping event.

h_c was measured using the capacitive wave gauge S10 which was located in the middle of the breakwater crest (see Figs. 2 and 3). S10 was inserted into a hollow cylinder (2 cm in length and 8.5 cm in diameter) filled with water so the sensor remained partially submerged.

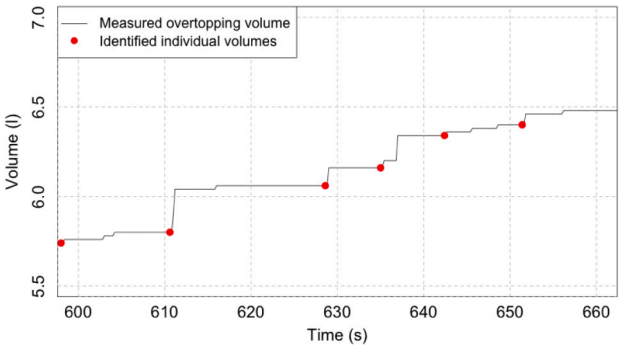

Fig. 4. Example of the collected overtopping volumes (test #1) and the beginning point of the identified individual wave overtopping events.

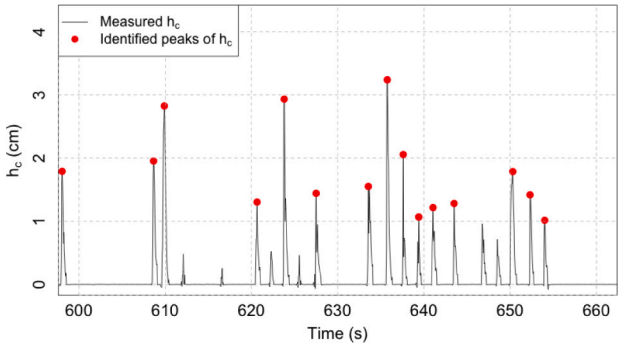

Fig. 5. Example of a recorded timeseries of h_c (test #1).

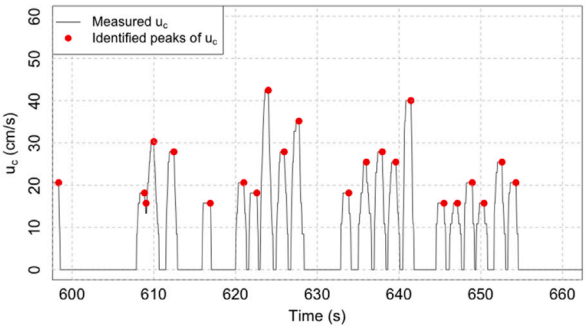

Fig. 6. Example of a recorded timeseries of u_c (test #1).

A lid with a slot was installed in the upper part to prevent water loss and to maintain the daily-calibrated reference level. Little variation in the reference level was seen and little noise was measured, as shown in Fig. 5. Peak values over 1 cm were extracted from the signal and considered for further analysis.

u_c was measured using three miniature propellers at a frequency of 20 Hz. Their operational range was $0.15 < u_c$ (m/s) < 3.00, so $u_c < 0.15$ m/s were disregarded. The three miniature propellers were installed along the crest: (1) on the seaward edge, (2) in the middle, and (3) on the leeward edge of the model crest. Here, measurements taken in the middle of the breakwater crest were used. Peak values within the operational range were considered for further analysis. An example timeseries is displayed in Fig. 6.

Once the individual wave overtopping events, V, and the peak values of h_c and u_c are extracted, concomitant events are assigned. This is, the values closer to each other in time are assigned as belonging to the same overtopping event. Note that V are recorded later due to the time that overtopping water needs to run through the chute and reach

the weighing system. Thus, those V closest in time to h_c and u_c but recorded later are assigned.

2.4. Dimensionless variables definition

This study is focused on the maximum overtopping layer thickness (h_c), the maximum overtopping flow velocity (u_c) and the individual wave overtopping volume (V) of each individual wave overtopping event. The following dimensionless expressions are considered here: h_c/H_{m0}, $u_c/\sqrt{gH_{m0}}$ and V/H_{m0}^2.

According to the literature, the explanatory variables which might influence h_c/H_{m0}, $u_c/\sqrt{gH_{m0}}$ and V/H_{m0}^2 are the bottom slope (m), the crest freeboard (R_c), the spectral significant wave height ($H_{m0} = 4\sqrt{m_0}$), the spectral wave period ($T_{m-1,0} = m_{-1}/m_0$) and water depth (h_s). These variables are made dimensionless as

- m, is the bottom slope, which determines the type of wave breaking at the toe of the structure. Moreover, in Mares-Nasarre et al. (2020a), the bottom slope m was found to play a significant role in the estimation of h_c and u_c.
- R_c/H_{m0}, is the dimensionless crest freeboard, which is the most widely accepted dimensionless variable that governs the mean wave overtopping discharge (e.g., Molines and Medina, 2016; van Gent et al., 2022). Moreover, it can be found in all methods in the literature to estimate V (e.g., Nørgaard et al., 2014; Mares-Nasarre et al., 2020b) and h_c and u_c (e.g., Mares-Nasarre et al., 2019, 2021).
- $s_{-1,0} = H_{m0}/L_{-1,0}$, is the wave steepness calculated with $L_{-1,0} = gT_{m-1,0}^2/2\pi$. This variable influences the wave breaking on the structure slope. $s_{-1,0}$ is included within the surf similarity parameter or Iribarren number ($Ir_{m-1,0}$, calculated with H_{m0} and the $T_{m-1,0}$) in methods to estimate V given by EurOtop (2018) and Koosheh et al. (2022). Also, it was reported as a significant explanatory variable to estimate h_c and u_c in studies such as Schüttrumpf and van Gent (2004) and Mares-Nasarre et al. (2019, 2021).
- h_s/H_{m0}, is the dimensionless water depth at the toe of the structure. This variable is used as an indicator of whether waves are depth-limited (van Gent, 1999; Nørgaard et al., 2014). Therefore, it can be found in the methods in the literature to estimate V (Nørgaard et al., 2014) and h_c and u_c (Mares-Nasarre et al., 2021).

3. Theoretical framework

In this study, a probabilistic model is proposed to describe the multivariate uncertainty of overtopping hydrodynamic variables. Parametric distribution functions are used to model the marginal distributions, while bivariate copulas are applied to describe the bivariate uncertainty between each pair of variables. In this section, the concepts of bivariate copula and tail dependence are introduced. Also, the goodness of fit criteria to assess the performance of copulas are presented.

3.1. Concept of bivariate copula

Bivariate copulas, or just copulas, are joint distributions with uniform marginal distributions in [0, 1]. According to Sklar (1959)'s theorem, any multivariate joint distribution of continuous variables can be described as a copula that models the dependence between the variables and a set of univariate marginal distributions. The definition of copula for the bivariate case is given by

$$H_{X_1,X_2}(x_1,x_2) = C\{F_{X_1}(x_1), G_{X_2}(x_2)\} \tag{2}$$

where $H_{X_1,X_2}(x_1,x_2)$ for $(x_1,x_2) \in \mathbb{R}^2$ is a joint distribution with marginals $F_{X_1}(x_1)$ and $G_{X_2}(x_2)$ in [0, 1] and a copula in the unit square $I^2 = ([0,1]\times[0,1])$, being Eq. (2) satisfied for all $(x_1,x_2) \in \mathbb{R}^2$.

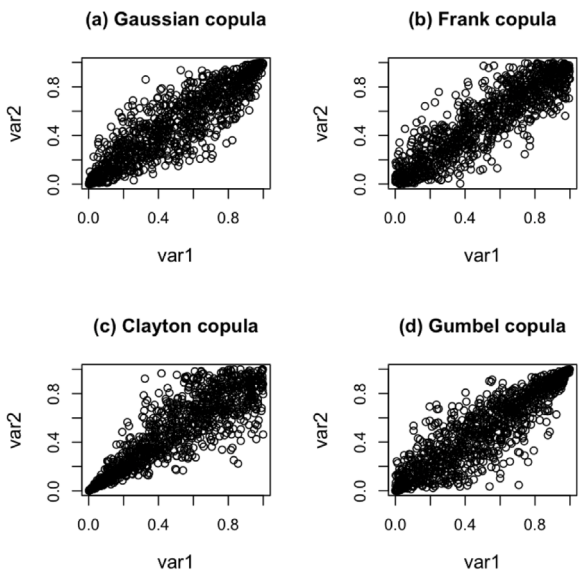

Fig. 7. Example of copula families with $r = 0.88$.

Different families of copulas can be found in the literature (see Czado, 2019); all families in R-library *VineCopula* by Nagler et al. (2022) are considered here. For further guidance on the application of copulas in maritime engineering, the reader is referred to Salvadori et al. (2014, 2015). One distinctive feature between copula families is tail dependence which characterizes the correlations in the tails of the distributions of two random variables. Thus, the upper tail dependence coefficient is defined as $\lambda_{upper} = \lim_{t\to 1^-} P(X_2 > F_2^{-1}(t) | X_1 > F_1^{-1}(t))$ (Sibuya et al., 1960; Joe, 1997). Note that calculating tail dependence in practical applications may lead to unreliable results for limited datasets (see more in Salvadori et al., 2007). Fig. 7 presents four common copula families with the same $r = 0.88$. Figs. 7(a) and (b) display the Gaussian and Frank copulas, which do not present tail dependence. Fig. 7(c) shows the Clayton copula, which presents lower tail dependence. This is, the lower values of the variables are more correlated than the higher values. Finally, Fig. 7(d) displays the Gumbel copula which presents upper tail dependence, so higher values of the random variables are more correlated than the lower ones. More about copulas can be found in Nelsen (2006).

3.2. Goodness of fit for bivariate copulas

For each test and pair of variables, the best copula model is investigated. The selection process is performed as follows. First, the best fitting copula in terms of Akaike Information Criterion, AIC (Akaike, 1973), in the R-library *VineCopula* by Nagler et al. (2022) is selected. Afterwards, the previously selected copula is compared with: (1) Gaussian, (2) Frank, (3) Clayton, and (4) Gumbel. The aforementioned comparison is performed using two criteria: (1) Cramer–von-Mises statistic (Genest et al., 2009), and (2) semi-correlations (Joe, 2014). When no clear tail dependence was observed as evaluated through the semi-correlations and the Cramer–von-Mises did not point out a given copula family as the best fitting copula, the Gaussian copula was selected for simplicity.

The Cramer–von-Mises statistic (S_{CvM}) assesses the distance between the empirical and the parametric copula. Thus, a perfect fit is given by $S_{CvM} \to 0$. In addition, an hypothesis test is performed and the p-value (p_{CvM}) is computed following the parametric bootstrap proposed in Genest et al. (2006). The null hypothesis of this test corresponds to the empirical and parametric copula coming from the same bivariate distribution. Therefore, $p_{CvM} < 0.05$ (significance level)

Table 2
Number of tests where each marginal distribution function provided the best fit.

Distr.	Gamma	Logn.	Norm.	Expon.	GEV	Rayl.
h_c/H_{m0}	**43**	36	23	0	16	0
$u_c/\sqrt{gH_{m0}}$	28	**65**	8	0	17	0
V/H_{m0}^2	17	**50**	0	31	15	5

Table 3
P-values for the two-samples Kolmogorov–Smirnov test applied to the parameters of the marginal distributions.

Parameter	h_c/H_{m0}		$u_c/\sqrt{gH_{m0}}$		V/H_{m0}^2	
	μ_h	σ_h	μ_u	σ_u	μ_V	σ_V
Cubes vs. Cubipod®	**0.01**	0.23	0.11	**0.03**	**0.04**	0.19

rejects the null hypothesis indicating a poor fit of the parametric copula.

Semicorrelations allow to assess whether a parametric copula is capturing the (presence or lack of) tail dependence in the data. This approach consists of transforming the pseudo-observations (observations in unity space) to standard normal space. There, four quadrants are delimited using $X = Y = 0$ and the correlations within those four quadrants are computed. This procedure is applied to both the empirical observations and the random samples obtained from the fitted parametric copula and the semicorrelations are compared.

4. Marginal distributions

4.1. Marginal distribution selection

In this section, the one-dimensional marginal distribution functions which better fit the observations of h_c/H_{m0}, $u_c/\sqrt{gH_{m0}}$ and V/H_{m0}^2 are identified. It should be noted that only those tests with at least 10 observations were included in the analysis. Six different distribution functions were considered: (1) Gamma, (2) Lognormal, (3) Normal, (4) Exponential, (5) Generalized Extreme Value (GEV), and (6) Rayleigh. For each test and variable, the six aforementioned distributions were fitted using Maximum Loglikelihood Estimator (MLE) and the best distribution in terms of AIC. Table 2 shows the number of tests where a given distribution function provided the best fit. Similar behavior is observed when splitting the number by armor elements, as shown in Appendix A.1.

In most cases, the Gamma distribution provided the best fit for h_c/H_{m0}, while the Lognormal distribution performed the best for $u_c/\sqrt{gH_{m0}}$ and V/H_{m0}^2. The Lognormal distribution was the second most frequently selected distribution for h_c/H_{m0} with a number close to that of the Gamma distribution. Gamma and Lognormal distributions are quite similar and both are widely used for describing positively skewed data. Thus, both Gamma and Lognormal distributions were considered to describe h_c/H_{m0}. In the subsequent sections, results for h_c/H_{m0} obtained with the Lognormal distribution function are presented, since it provided the best results in the following phases of the analysis.

The cumulative distribution function of the Lognormal distribution is given by

$$F(x) = \frac{1}{2}\left[1 + erf\left(\frac{ln(x) - \mu}{\sqrt{2}\sigma}\right)\right] \tag{3}$$

where erf denotes the error function, and μ and σ are the mean and the standard deviation of the variable's natural logarithm. If X follows a Lognormal distribution, $Y = ln(X)$ follows a Normal distribution.

4.2. Marginal distribution fitting

After selecting the best fitting distributions in the previous section, they were fitted to each variable and test using MLE. The goodness of fit of the Lognormal distribution was assessed using both the one-sample Kolmogorov–Smirnov (Kolmogorov, 1933; Smirnov, 1948) and the one-sample Anderson–Darling (Anderson and Darling, 1952, 1954) hypothesis tests. The null hypothesis of these tests is that the samples come from the given distribution. Thus, $p-values$ below the significance level (here, 0.05) indicate a statistically significant difference. The Lognormal distribution could not be rejected as a valid model in 99% of the cases using the Kolmogorov–Smirnov test, while in all the tests it could not be rejected as a valid model according to the Anderson–Darling test.

Once fitted for each variable and test, the obtained parameters were analyzed. First, the existence of significant differences between the parameters obtained for the different armor elements was assessed using the two-samples Kolmogorov–Smirnov test. The null hypothesis is that both samples come from the same distribution. Thus, $p-values$ below the significance level (here, 0.05) indicate a statistically significant difference. Since few tests of the double-layer randomly-placed rock-armored model presented a sufficient number of observations of h_c/H_{m0}, $u_c/\sqrt{gH_{m0}}$ or V/H_{m0}^2, the comparison was performed between the single-layer Cubipod®-armored and the double-layer randomly-placed cube-armored models. As shown in Table 3, three out of six possible differences between the two types of armor layers were found significant. However, two of those $p-values$ are close to the significance level of 0.05, so no significant difference between the armor elements was assumed.

4.3. Formulas for the parameters of the marginal distributions

In the subsequent sections, formulas to estimate the parameters of the lognormal distributions to model h_c/H_{m0}, $u_c/\sqrt{gH_{m0}}$ and V/H_{m0}^2 as function of the explanatory variables defined in Section 2.4 are developed. The methodology to do so is as follows:

- Parameters are plotted against the explanatory variables and formulas are proposed based on the observed relationships. When no clear shape is observed, a linear relationship is proposed.
- Data is randomly divided into two subsets: (1) training subset (70% data), and (2) test subset (30% data). Data in the training subset is used to fit the model, while data in the test subset is used to assess the performance of the model after the fitting process.
- Linear regression is performed with the data on the training subset to determine which explanatory variables in Section 2.4 are significant, as well as to fit the coefficients.

4.3.1. Lognormal distribution for h_c/H_{m0}

In this section, the parameters of the Lognormal distribution to describe h_c/H_{m0}, denoted here as μ_h and σ_h, are studied. Fig. 17 in Appendix A.2 presents the influence of the explanatory variables on the parameter μ_h. A linear relationship is observed between μ_h and the explanatory variables. Thus, Eq. (4) is proposed to estimate μ_h.

$$\mu_h = A_1\ m + A_2\left(\frac{R_c}{H_{m0}}\right) + A_3 s_{-1,0} + A_4\frac{h_s}{H_{m0}} + A_5 \tag{4}$$

where A_1, A_2, A_3, A_4 and A_5 are coefficients to be fitted. Following methodology in 4.3, all variables were found significant with $A_1 = -13$, $A_2 = -0.2$, $A_3 = -13$, $A_4 = 0.5$ and $A_5 = -1.6$. Note that the higher the μ_h, the higher the predicted values of h_c/H_{m0}. Therefore, according to Eq. (4), the lower the m, the R_c/H_{m0} or the $s_{-1,0}$, the higher the h_c/H_{m0}, in accordance with Mares-Nasarre et al. (2020a, 2021). On the other hand, deeper waters (higher h_s/H_{m0}) lead to higher predicted h_c/H_{m0}. The validity ranges for Eq. (4) are $0.02 \le m \le 0.04$, $0.35 \le R_c/H_{m0} \le 1.73$, $0.015 \le s_{-1,0} \le 0.057$, $1.27 \le h_s/H_{m0} \le 3.24$ and $-2.33 \le \mu_h \le -0.92$. The performance of the formula is reasonable with $R^2 = 0.59$ in the testing subset. Fig. 8 presents the comparison between the observed and estimated μ_h using the fitted Eq. (4), as well as the 90% error band.

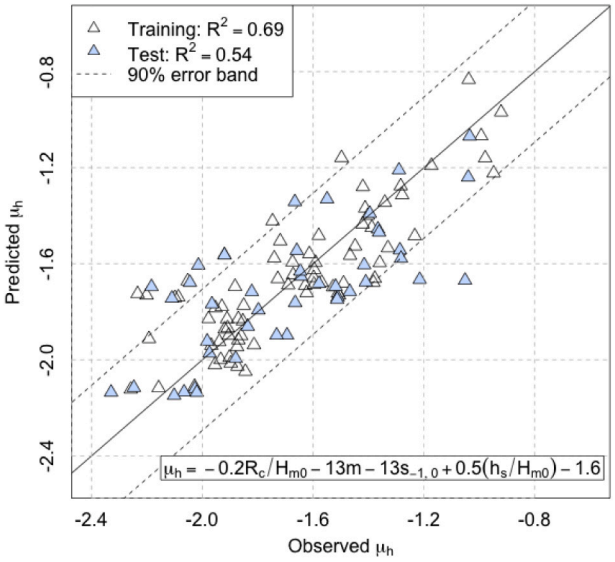

Fig. 8. Comparison between the observed and estimated μ_h using Eq. (4) with $A_1 = -13$, $A_2 = -0.2$, $A_3 = -13$, $A_4 = 0.5$ and $A_5 = -1.6$.

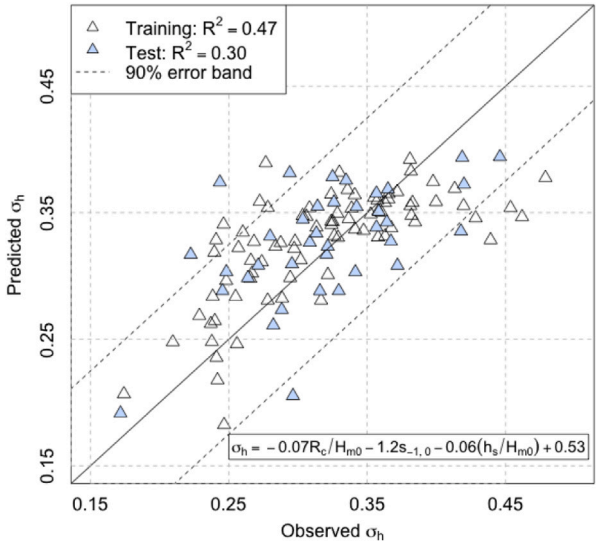

Fig. 9. Comparison between the observed and estimated σ_h using Eq. (6) with $B_1 = 0$, $B_2 = -0.07$, $B_3 = -1.2$, $B_4 = -0.06$ and $B_5 = 0.53$.

Assuming a Gaussian error distribution, the 90% error band is given by

$$\mu_h\Big|_{5\%}^{95\%} = \mu_h \pm 1.64\sqrt{var(\epsilon)} = \mu_h \pm 0.29 \tag{5}$$

Fig. 18 in Appendix A.2 presents the influence of the explanatory variables defined in Section 2.4 on the parameter σ_h. No clear shape of the dependence between σ_h and the explanatory variables is observed, so a linear relationship proposed in Eq. (6).

$$\sigma_h = B_1\ m + B_2\left(\frac{R_c}{H_{m0}}\right) + B_3 s_{-1,0} + B_4\frac{h_s}{H_{m0}} + B_5 \tag{6}$$

where B_1, B_2, B_3, B_4 and B_5 are coefficients to be fitted. m was not found significant, so $B_1 = 0$, $B_2 = -0.07$, $B_3 = -1.2$, $B_4 = -0.06$ and $B_5 = 0.53$. Note that the higher the σ_h, the wider the distribution of h_c/H_{m0} and the longer the tail, so higher values of h_c/H_{m0} become more likely. Therefore, the lower the R_c/H_{m0}, the $s_{-1,0}$ and h_s/H_{m0} (shallower waters), the higher probability of observing extreme values of h_c/H_{m0}. The experimental ranges for Eq. (6) are $0.35 \le R_c/H_{m0} \le 1.73$, $0.015 \le s_{-1,0} \le 0.057$, $1.27 \le h_s/H_{m0} \le 3.24$ and $0.17 \le \sigma_h \le 0.48$. The developed formula presents a reasonable performance with $R^2 = 0.30$ in the testing subset. Fig. 9 compares the observed and estimated σ_h using the fitted Eq. (6). The 90% error band is also presented.

Assuming a Gaussian error distribution, the 90% error band is computed as

$$\sigma_h\Big|_{5\%}^{95\%} = \sigma_h \pm 0.075 \tag{7}$$

4.3.2. Lognormal distribution for $u_c/\sqrt{gH_{m0}}$

Parameters of the Lognormal distribution to describe $u_c/\sqrt{gH_{m0}}$, denoted here as μ_u and σ_u, are analyzed. The variability of μ_u was very low, with a mean value of −1.485 and a standard deviation of 0.104. Moreover, no clear influence of the explanatory variables was found on the parameters μ_u, as shown in Figs. 19 and 20 in Appendix A.2. Consequently, $\mu_u = -1.5$ is recommended here.

Fig. 21 in Appendix A.2 shows the influence of the explanatory variables on the parameter σ_u. No clear influence of $s_{-1,0}$, R_c/H_{m0} or m is observed on σ_u, while a negative linear relationship between h_s/H_{m0} and σ_u is observed. Thus, Eq. (8) is proposed to predict σ_u.

$$\sigma_u = C_1\ m + C_2\left(\frac{R_c}{H_{m0}}\right) + C_3 s_{-1,0} + C_4\frac{h_s}{H_{m0}} + C_5 \tag{8}$$

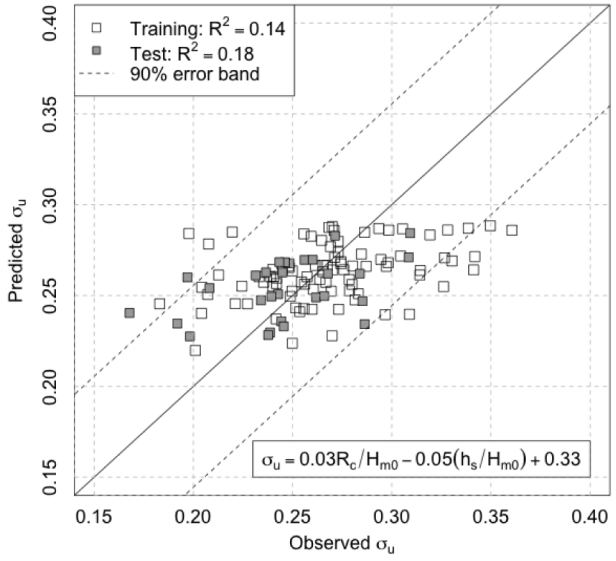

Fig. 10. Comparison between the observed and estimated σ_u using Eq. (8) with $C_1 = 0$, $C_2 = 0.03$, $C_3 = 0$, $C_4 = -0.05$ and $C_5 = 0.33$.

where C_1, C_2, C_3, C_4 and C_5 are coefficients to be fitted. Only R_c/H_{m0} and h_s/H_{m0} were found significant, so $C_1 = 0$, $C_2 = 0.03$, $C_3 = 0$, $C_4 = -0.05$ and $C_5 = 0.33$. Note that the higher the σ_u, the wider the distribution of $u_c/\sqrt{gH_{m0}}$, so the longer the tail and higher values of $u_c/\sqrt{gH_{m0}}$ become more likely. Therefore, the higher R_c/H_{m0} and the shallower waters (lower h_s/H_{m0}), the wider the distribution of $u_c/\sqrt{gH_{m0}}$ and, thus, higher extremes of $u_c/\sqrt{gH_{m0}}$ are expected. The validity ranges for Eq. (8) are $0.35 \le R_c/H_{m0} \le 1.73$, $1.27 \le h_s/H_{m0} \le 3.24$ and $0.17 \le \sigma_u \le 0.36$. The proposed formula presents a reasonable performance with $R^2 = 0.18$ in the testing subset. Fig. 10 compares the observed and estimated σ_u using the fitted Eq. (8). The 90% error band is also presented.

Assuming a Gaussian error distribution, the 90% error band can be estimated as

$$\sigma_u\Big|_{5\%}^{95\%} = \sigma_u \pm 0.06 \tag{9}$$

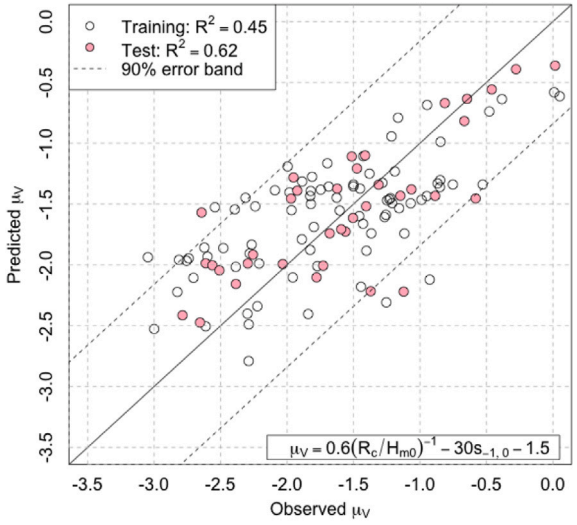

Fig. 11. Comparison between the observed and estimated μ_V using Eq. (10) with $D_1 = 0$, $D_2 = 0.6$, $D_3 = -30$, $D_4 = 0$ and $D_5 = -1.5$.

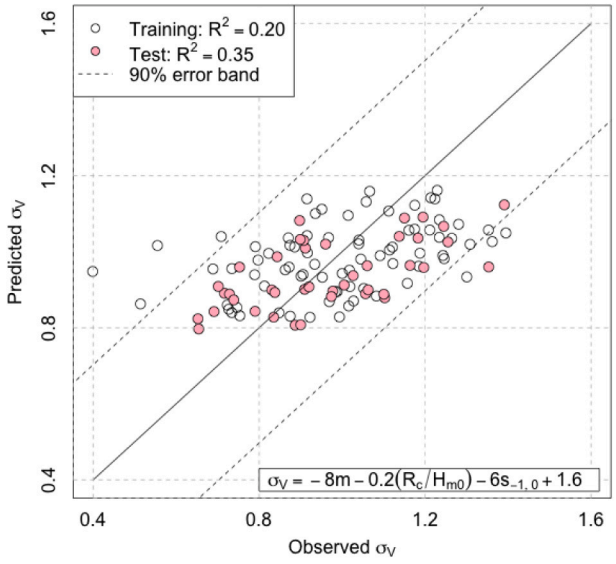

Fig. 12. Comparison between the observed and estimated σ_V using Eq. (12) with $E_1 = -8$, $E_2 = -0.2$, $E_3 = -6$, $E_4 = 0$ and $E_5 = 1.6$.

4.3.3. Lognormal distribution for V/H_{m0}^2

In this section, predictors for the parameters of the Lognormal distribution to describe V/H_{m0}^2, denoted here as μ_V and σ_V, are derived. Fig. 22 in Appendix A.2 presents the influence of the explanatory variables defined in Section 2.4 on the parameter μ_V. It is shown how lower values of $s_{-1,0}$ lead to higher values of μ_V. Also, a negative power law between R_c/H_{m0} and μ_V is observed. Thus, Eq. (10) is proposed to predict μ_V.

$$\mu_V = D_1\, m + D_2 \left(\frac{R_c}{H_{m0}}\right)^{-1} + D_3 s_{-1,0} + D_4 \frac{h_s}{H_{m0}} + D_5 \tag{10}$$

where D_1, D_2, D_3, D_4 and D_5 are coefficients to be fitted. m was found not relevant, in accordance with previous studies (Mares-Nasarre et al., 2020b), together with h_s/H_{m0}. Therefore, $D_1 = 0$, $D_2 = 0.6$, $D_3 = -30$, $D_4 = 0$ and $D_5 = -1.5$. Note that the higher the μ_V, the higher the predicted values of V/H_{m0}^2. Thus, the higher the $s_{-1,0}$ and the lower the R_c/H_{m0}, the higher the V/H_{m0}^2. This is in agreement with previous studies such as Molines and Medina (2016) or Koosheh et al. (2021). The experimental ranges for Eq. (10) are $0.35 \le R_c/H_{m0} \le 1.73$, $0.015 \le s_{-1,0} \le 0.057$ and $-3.05 \le \mu_V \le 0.05$. The developed formula presents a good performance with $R^2 = 0.62$ in the testing subset. Fig. 11 presents the comparison between the observed and estimated μ_V using the fitted Eq. (10), as well as the 90% error band.

Assuming a Gaussian error distribution, the 90% error band can be estimated as

$$\mu_V \Big|_{5\%}^{95\%} = \mu_V \pm 0.84 \tag{11}$$

Fig. 23 in Appendix A.2 presents the influence of the explanatory variables in Section 2.4 on the parameter σ_V. No clear relationship was observed between σ_V and the explanatory variables, so Eq. (12) is proposed for its prediction.

$$\sigma_V = E_1\, m + E_2 \left(\frac{R_c}{H_{m0}}\right) + E_3 s_{-1,0} + E_4 \frac{h_s}{H_{m0}} + E_5 \tag{12}$$

where E_1, E_2, E_3, E_4 and E_5 are coefficients to be fitted. h_s/H_{m0} was found not relevant, so $E_1 = -8$, $E_2 = -0.2$, $E_3 = -6$, $E_4 = 0$ and $E_5 = 1.6$. This result points out that wave breaking may not have a major influence on the distribution of the individual wave overtopping volumes, as found in Mares-Nasarre et al. (2020b). Note that the higher the σ_V, the wider the distribution, so higher values of V/H_{m0}^2 become more likely. Therefore, according to Eq. (12), lower values of $s_{-1,0}$ and R_c/H_{m0} lead to higher values of σ_V and, thus, the more likely the extreme values of V/H_{m0}^2. These observations are in agreement with previous literature (Molines and Medina, 2016; Koosheh et al., 2021). The experimental ranges for Eq. (12) are $0.02 \le m \le 0.04$, $0.35 \le R_c/H_{m0} \le 1.73$, $0.015 \le s_{-1,0} \le 0.057$ and $0.40 \le \sigma_V \le 1.39$. The developed formula presents a reasonable performance with $R^2 = 0.35$ in the testing subset. Fig. 12 compares the observed and estimated σ_V using the fitted Eq. (12). The 90% error band is also shown.

Assuming a Gaussian error distribution, the 90% error band is given by

$$\sigma_V \Big|_{5\%}^{95\%} = \mu_V \pm 0.30 \tag{13}$$

4.4. Marginal distributions performance

Once the marginal distributions h_c/H_{m0}, $u_c/\sqrt{gH_{m0}}$ and V/H_{m0}^2 are defined and their parameters are fitted, the overall performance of the models is assessed here. To do so, the observed quantiles h_c/H_{m0}, $u_c/\sqrt{gH_{m0}}$ and V/H_{m0}^2 are compared to the predicted quantiles using the models developed in the previous sections. A satisfactory performance of the proposed distributions is observed with $0.67 \le R^2 \le 0.78$. As an example, the comparison between the measured and estimated quantiles of V/H_{m0}^2 is shown in Fig. 13. Note that Fig. 13 is displayed in logarithmic scale and that each color in the plots represent a different test. In Appendix A.3, the comparison between the measured and predicted quantiles for h_c/H_{m0} and $u_c/\sqrt{gH_{m0}}$ is shown in Figs. 24 and 25. Also, 90% error bands are shown in Figs. 24, 25 and 13.

The 90% error band for h_c/H_{m0}, $u_c/\sqrt{gH_{m0}}$ and V/H_{m0}^2 is calculated following the methodology in Herrera and Medina (2015). A Gaussian error distribution of the error (ε) is assumed, with 0 mean and the variances given by

$$var(\varepsilon_h) = 0.03(h_c/H_{m0})^2 \tag{14}$$

$$var(\varepsilon_u) = 0.017(u_c/\sqrt{gH_{m0}})^2 \tag{15}$$

$$var(\varepsilon_V) = 0.15(V/H_{m0}^2)^2 \tag{16}$$

Thus, the 90% error bands are computed as

$$h_c/H_{m0} \Big|_{5\%}^{95\%} = h_c/H_{m0} \pm 1.64\sqrt{0.03(h_c/H_{m0})^2} \tag{17}$$

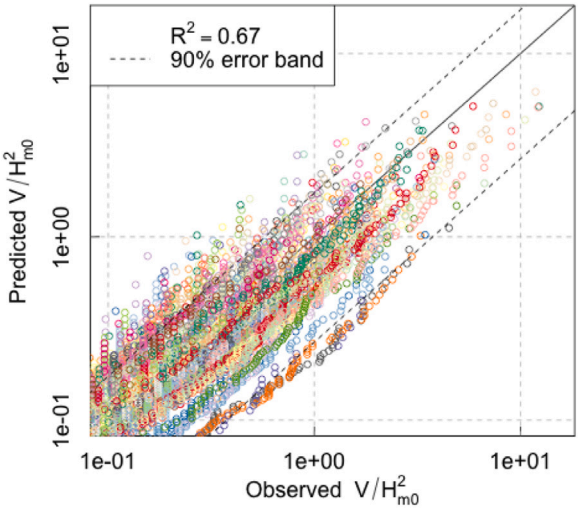

Fig. 13. Comparison between the measured and estimated V/H_{m0}^2 marginal distributions with Lognormal distribution in Eq. (3) and parameters in Eqs. (10) and (12).

Table 4
Best fit copulas for all pairs with significant rank correlation.

Copula	Gaussian	Frank	Clayton	Gumbel	Other
$h_c/H_{m0} - u_c/\sqrt{gH_{m0}}$	**8**	2	6	6	4
$h_c/H_{m0} - V/H_{m0}^2$	18	11	**23**	18	6
$V/H_{m0}^2 - u_c/\sqrt{gH_{m0}}$	0	4	8	**11**	0

$$u_c/\sqrt{gH_{m0}}\Big|_{5\%}^{95\%} = u_c/\sqrt{gH_{m0}} \pm 1.64\sqrt{0.017(u_c/\sqrt{gH_{m0}})^2} \tag{18}$$

$$V/H_{m0}^2\Big|_{5\%}^{95\%} = V/H_{m0}^2 \pm 1.64\sqrt{0.15(V/H_{m0}^2)^2} \tag{19}$$

5. Copula model

5.1. Copula selection

In this section, the bivariate copulas which better model the dependence between h_c/H_{m0}, $u_c/\sqrt{gH_{m0}}$ and V/H_{m0}^2 are identified. It should be noted that only those tests with at least 20 observations and a significant r (see Eq. (25)) are considered; $p-values < 0.05$ indicate a significant r. Figs. 26 and 27 in Appendix B.1 present the values of r, as well as their associated $p-values$.

As explained in 3.2, for each test and pair of variables, the following copula families are compared: (1) Gaussian, (2) Frank, (3) Clayton, (4) Gumbel, and (5) the best fitting copula in terms of AIC within those included in the R-library *VineCopula* by Nagler et al. (2022). Those copulas are compared using Cramer–von-Mises statistic and semi-correlations. Further information about the selection procedure is given in 3.2. Table 4 summarizes the copulas selected for each pair of variables.

In most cases, the best fit for $h_c/H_{m0} - u_c/\sqrt{gH_{m0}}$ was the Gaussian copula. Moreover, no clear tail dependence was observed, so the Gaussian copula is an appropriate model. For the pair $h_c/H_{m0} - V/H_{m0}^2$, the best fit in most tests is the Clayton copula. In addition, 3 out of the 6 other copulas lead to the Survival Gumbel, which also presents a lower tail dependence. Finally, the best fit for the pair $V/H_{m0}^2 - u_c/\sqrt{gH_{m0}}$ was the Gumbel copula. Equations for the selected copulas are given in B.2. Note that for the selected copula models it holds that $C\{F_{X_1}(x_1), G_{X_2}(x_2)\} = C\{G_{X_2}(x_2), F_{X_1}(x_1)\}$.

Tables 9–11 in Appendix B.3 show the fitting results divided by armor element. It is shown how Gaussian and Gumbel copulas are again the best fit for the pairs $h_c/H_{m0} - u_c/\sqrt{gH_{m0}}$ and $V/H_{m0}^2 - u_c/\sqrt{gH_{m0}}$, respectively, independently of the armor. Regarding the pair $h_c/H_{m0} - V/H_{m0}^2$, the selected Clayton copula is the best fit for the single-layer Cubipod®armor data and the second best for the double-layer randomly-placed cube armor data. Only 6 tests are available for rock armors. Consequently, it is considered that no significant differences in the copula selection arise from the different armors.

Table 5
P-values for the two-samples Kolmogorov–Smirnov test applied to the parameters of the copulas.

	Gaussian	Clayton	Gumbel
Parameter	ρ_{hu}	δ_{hV}	θ_{Vu}
Cubes vs. Cubipod®	0.83	0.99	0.16

5.2. Copula fitting

Once best fitting copulas for each pair of variables are selected, the selected copula for each variable is fitted using MLE and the fitted parameters are analyzed.

Similarly to Section 4.2, the existence of significant differences between the parameters for the different armor elements is assessed using the two-samples Kolmogorov–Smirnov test (Kolmogorov, 1933; Smirnov, 1948). Again, the comparison is performed between the single-layer Cubipod®-armored and the double-layer randomly-placed cube-armored models, since few tests of the double-layer randomly-placed rock-armored model present a sufficient number of observations. As shown in Table 5, no significant differences were observed.

5.2.1. Gaussian copula for h_c/H_{m0} and $u_c/\sqrt{gH_{m0}}$

In this section, the parameter of the Gaussian copula to describe the dependence structure of the pair h_c/H_{m0} and $u_c/\sqrt{gH_{m0}}$, denoted here as ρ_{hu}, is analyzed. Fig. 28 presents the influence of the explanatory variables defined in Section 2.4 on the parameter ρ_{hu}. Eq. (20) is proposed to explain ρ_{hu}.

$$\rho_{hu} = G_1 m + G_2\left(\frac{R_c}{H_{m0}}\right) + G_3 s_{-1,0} + G_4\frac{h_s}{H_{m0}} + G_5 \tag{20}$$

where G_1, G_2, G_3, G_4 and G_5 are coefficients to be fitted. Data is randomly divided into a training (70% data), and a test subset (30% data). Linear regression is performed with Eq. (20) and the data on the training subset to determine which variables are significant, as well as to fit the coefficients. As expected, only h_s/H_{m0} was found significant, so $G_1 = 0$, $G_2 = 0$, $G_3 = 0$, $G_4 = 0.22$ and $G_5 = 0$. Thus, deeper water (higher h_s/H_{m0}) leads to higher correlation between h_c/H_{m0} and $u_c/\sqrt{gH_{m0}}$. The experimental ranges for Eq. (20) are $1.27 \le h_s/H_{m0} \le 2.77$ and $0.23 \le \rho_{hu} \le 0.72$. Note that only experiments with a significant r were included in the bivariate analysis, as explain in Section 5.1. The performance of the formula is reasonable with $R^2 = 0.52$ in the testing subset. Fig. 14 presents the comparison between the observed and estimated ρ_{hu} using the fitted Eq. (20), as well as the 90% error band.

Assuming a Gaussian error distribution, the 90% error band is given by

$$\rho_{hu}\Big|_{5\%}^{95\%} = \mu_h \pm 0.18 \tag{21}$$

5.2.2. Clayton copula for h_c/H_{m0} and V/H_{m0}^2

Here, the parameter of the Clayton copula to model the dependence of the pair h_c/H_{m0} and V/H_{m0}^2, denoted here as δ_{hV}, is analyzed. No clear influence of the explanatory variables on δ_{hV} was found, as shown in Fig. 29 in Appendix B.4. Therefore, $\delta_{hV} = 0.8$ was suggested. Note that this means that a constant value of the correlation between h_c/H_{m0} and V/H_{m0}^2 can be assumed. This is valid within the experimental ranges $0.02 \le m \le 0.04$, $0.34 \le R_c/H_{m0} \le 1.25$, $0.015 \le s_{-1,0} \le 0.057$ and $1.28 \le h_s/H_{m0} \le 3.24$.

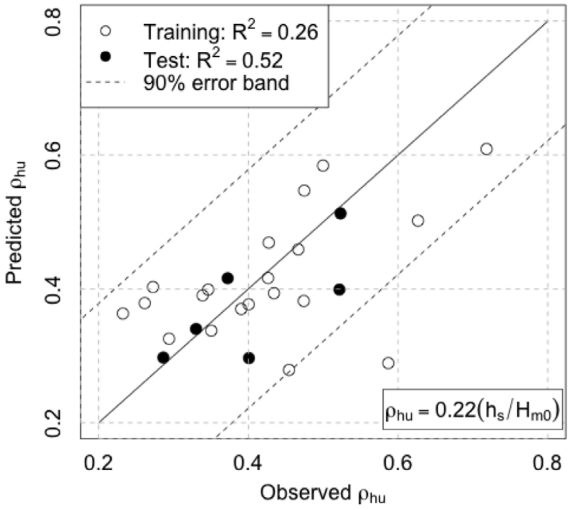

Fig. 14. Comparison between the observed and estimated ρ_{hu} using Eq. (20) with $G_1 = 0$, $G_2 = 0$, $G_3 = 0$, $G_4 = 0.21$ and $G_5 = 0$.

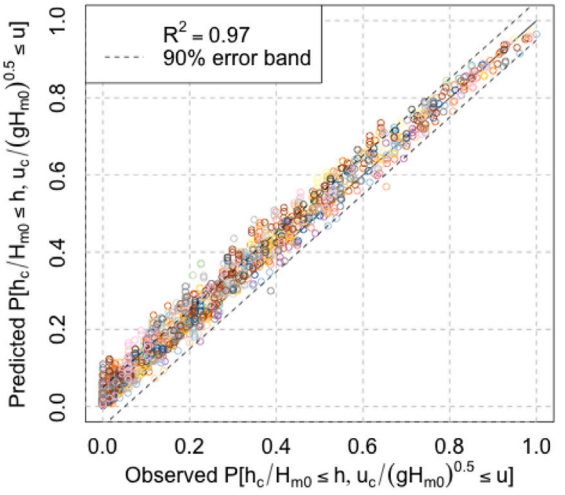

Fig. 15. Comparison between the observed and estimated non-exceedance joint probabilities for the pair h_c/H_{m0} and $u_c/\sqrt{gH_{m0}}$.

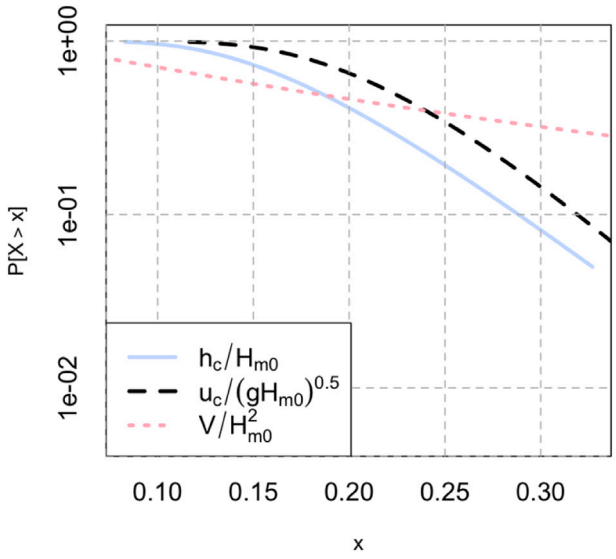

Fig. 16. Exceedance probability plot for the predicted marginal distributions of h_c/H_{m0}, $u_c/\sqrt{gH_{m0}}$, and V/H_{m0}^2.

5.2.3. Gumbel copula for V/H_{m0}^2 and $u_c/\sqrt{gH_{m0}}$

Here, the parameter of the Gumbel copula used to describe the dependence between the pair V/H_{m0}^2 and $u_c/\sqrt{gH_{m0}}$, denoted here as θ_{Vu}, is analyzed. No clear influence of the explanatory variables on θ_{Vu} was observed, as displayed in Fig. 30 in Appendix B.4. Thus, $\theta_{Vu} = 1.2$ was suggested here. Note that this means that a constant value of the rank correlation between V/H_{m0}^2 and $u_c/\sqrt{gH_{m0}}$ can be assumed. Its validity ranges are $0.02 \leq m \leq 0.04$, $0.34 \leq R_c/H_{m0} \leq 0.85$, $0.015 \leq s_{-1,0} \leq 0.048$ and $1.27 \leq h_s/H_{m0} \leq 2.49$.

5.3. Copula performance

Once the copula models for the pairs h_c/H_{m0} and $u_c/\sqrt{gH_{m0}}$, h_c/H_{m0} and V/H_{m0}^2 and V/H_{m0}^2 and $u_c/\sqrt{gH_{m0}}$ are selected and their parameters are fitted, the overall performance of the models is assessed here. To do so, the empirical joint non-exceedance probabilities for the observed values of h_c/H_{m0}, $u_c/\sqrt{gH_{m0}}$ and V/H_{m0}^2 are compared to the non-exceedance probabilities computed with the developed probabilistic models in the previous sections. A satisfactory performance is observed with $0.97 \leq R^2 \leq 0.98$. As an example, the comparison between the observed and estimated joint non-exceedance probabilities the pair h_c/H_{m0} and $u_c/\sqrt{gH_{m0}}$ is shown in Fig. 15. In Appendix B.5, the comparison for the pairs h_c/H_{m0} and V/H_{m0}^2 and V/H_{m0}^2 and $u_c/\sqrt{gH_{m0}}$ is presented in Figs. 31 and 32, respectively. Also, 90% error bands are presented. The 90% error bands are computed similarly to previous sections, so they are given by

$$P[h_c/H_{m0} \leq h, u_c/\sqrt{gH_{m0}} \leq u]\Big|_{5\%}^{95\%} = P[h_c/H_{m0} \leq h, u_c/\sqrt{gH_{m0}} \leq u] \pm 0.05 \tag{22}$$

$$P[h_c/H_{m0} \leq h, V/H_{m0}^2 \leq v]\Big|_{5\%}^{95\%} = P[h_c/H_{m0} \leq h, V/H_{m0}^2 \leq v] \pm 0.05 \tag{23}$$

$$P[V/H_{m0}^2 \leq v, u_c/\sqrt{gH_{m0}} \leq u]\Big|_{5\%}^{95\%} = P[V/H_{m0}^2 \leq v, u_c/\sqrt{gH_{m0}} \leq u] \pm 0.05 \tag{24}$$

6. Example of application and recommendations of use

In this section, an example is given on how to apply the developed probabilistic model to better design the crest level of a mound breakwater. The following methodology is illustrated in Fig. 1. Here, a mound breakwater placed on a gentle sea bottom ($m = 0.02$) is considered, facing a storm that can be characterized by $H_{m0} = 5$ m and $T_{m-1,0} = 10$ s, so $s_{-1,0} = 0.032$. The structure is placed at $h_s = 7.5$ m, and presents a $R_c = 4$ m, so $h_s/H_{m0} = 1.5$ and $R_c/H_{m0} = 0.8$.

Applying the results in Section 4.3, the marginal distributions of h_c/H_{m0}, $u_c/\sqrt{gH_{m0}}$ and V/H_{m0}^2 are modeled by Lognormal distributions with parameters $\mu_h = -1.69$ and $\sigma_h = 0.35$, $\mu_u = -1.5$ and $\sigma_u = 0.28$, and $\mu_V = -1.71$ and $\sigma_V = 1.09$, respectively. Fig. 16 shows the exceedance probability plots of the predicted marginals.

Different tolerability limits for h_c, u_c and V can be found in literature (e.g., Geeraerts et al., 2007; Bae et al., 2016), which need to be carefully selected for each location. In order to illustrate the use of the model, the following tolerability limits are selected: $h_c = 1$ m, $u_c = 2$ m/s and $V = 2 \cdot 10^3$ l/m. Thus, $h_c/H_{m0} = 0.2$, $u_c/\sqrt{gH_{m0}} = 0.29$ and $V/H_{m0}^2 = 0.08$. These values correspond to univariate exceedance probabilities of 0.41, 0.19 and 0.77, respectively. Thus, for the considered limits and boundary conditions, the tolerability limit for $V/H_{m0}^2 = 0.08$ is the most restrictive since it is the most likely to be exceeded. It should be noted that this reasoning is possible since

the same axiomatic probability is used for the three studied variables, different from previous literature.

In order to assess the safety of the structure against the overtopping failure mode, the probability of not fulfilling at least one of the tolerability limits needs to be computed. This can be done assuming the independence between the variables (only marginal distributions needed) or accounting for the dependence between the variables (both marginal distributions and dependence model needed). Here, the probability of not fulfilling at least one of the limits is computed under and without the independence assumption to compare the results later on.

In order to compute the joint exceedance probability of the tolerability limits, the following use of the developed model is recommended. Each bivariate copula models the joint probabilities of two variables. Thus, using only two out of the three copula models is enough to calculate the joint probability of the three variables ($X_1-X_2-X_3$). Here, it is recommended to use the Clayton copula for h_c/H_{m0} and V/H_{m0}^2 in Section 5.2.2 with $\delta_{hV} = 0.8$ and the Gumbel copula for V/H_{m0}^2 and $u_c/\sqrt{gH_{m0}}$ in Section 5.2.3 with $\theta_{Vu} = 1.2$. This is because Clayton and Gumbel copulas present tail dependence, while the Gaussian copula selected for the pair h_c/H_{m0} and $u_c/\sqrt{gH_{m0}}$ is the most generic model. Thus, it is suggested here to ensure that the tail dependence is included in the predictions while the generic dependence is left to the inference between the other two. Note that this proposal resembles a one-tree vine-copula, which assumes the conditional independence between the variables (for further information the reader is referred to Czado, 2019).

Here, an algorithm to calculate the joint probabilities using the described model following a Monte Carlo approach is recommended. However, this could also be done by numerical integration. The suggested algorithm is as follows:

1. The tolerability limits of the variables are transformed to unity space using the marginal distributions: $h_{lim} = 0.59$, $u_{lim} = 0.81$ and $V_{lim} = 0.23$.
2. Three random samples of size N in $[0, 1]$ are drawn from a uniform distribution, denoted as S_1, S_2 and S_3. Here, $N = 5000$ is used to illustrate the process.
3. S_1 represent random samples of h_c, while S_2 represent the conditional probabilities $F(V|h_c)$. Therefore, the values of V corresponding to S_1 and S_2 (S_V) can be computed using the inverse of the conditional distribution function of the Clayton copula. The inverse conditional distribution functions for different copula families can be found in Aas et al. (2009) denoted as the inverse of the h-functions.
4. S_3 represent the conditional probabilities $F(u_c|V)$. Then, the samples of u_c (S_u) are computed using the inverse of the conditional distribution function of the Gumbel copula with S_3 and S_V.
5. $S_1 = S_h$, S_u and S_V are random samples in unity space of h_c/H_{m0}, $u_c/\sqrt{gH_{m0}}$, and V/H_{m0}^2 which account for the dependence between them. The number of samples which do not fulfill at least one of the three tolerability limits (h_{lim}, u_{lim} and V_{lim}) defined in Step 1 is counted, N_f.
6. The probability of not fulfilling at least one tolerability limit is then computed as $P[h_c/H_{m0} > h_{lim}\ OR\ u_c/\sqrt{gH_{m0}} > u_{lim}\ OR\ V/H_{m0}^2 > V_{lim}] = N_f/N$.

Using the described procedure, the $P[h_c/H_{m0} > h_{lim}\ OR\ u_c/\sqrt{gH_{m0}} > u_{lim}\ OR\ V/H_{m0}^2 > V_{lim}] = 0.83$. If the dependence between the variables is neglected and, thus, independence between the variables is assumed $P[h_c/H_{m0} > h_{lim}\ OR\ u_c/\sqrt{gH_{m0}} > u_{lim}\ OR\ V/H_{m0}^2 > V_{lim}] = 0.89$. Thus, if dependence between the variables is considered, the obtained probability of failure against overtopping is lower, giving room for optimizing the structure. A lower crest freeboard can be then designed and, thus, less visual and environmental impacts (lower material consumption) are derived from the mound breakwater construction.

This section has shown one example of application of the developed model, although there are others. For instance, if the value of one variable is known, the conditionalized distribution of the other two given this observation can be computed, giving insight into the physical interaction between them.

7. Conclusions and recommendations

Consequences of climate change, namely sea level rise and stronger wave conditions, and the social pressure to diminish the visual impact of coastal structures lead to an increase of the overtopping hazard on coastal structures. Safety of coastal structures against overtopping can be assessed through the hydrodynamic variables which describe the individual wave overtopping events: the overtopping layer thickness (h_c), the overtopping flow velocity (u_c) and the individual wave overtopping volume (V). Models in the literature to characterize those variables present several limitations, since they are deterministic and/or they involve a chain of subsequent estimations leading to accumulated errors. Moreover, they do not allow to compute the probability if criteria are set to more than one of the overtopping variables (OR probability), since they do not account for the dependence between them.

In this study, a probabilistic model based on bivariate copulas is proposed to describe the joint probability distribution of h_c, u_c and V and, thus, account for the dependence between them. This model was built using experimental data from Mares-Nasarre et al. (2021). Tests were performed with relatively deep water to depth-limited wave conditions ($1.25 \leq h_s/H_{m0} \leq 5.00$), with two mild bottom slopes ($m = 2\%$ and 4%) and a wide range of dimensionless crest freeboards ($0.33 \leq R_c/H_{m0} \leq 3.20$).

Lognormal distribution functions are proposed to describe the univariate uncertainty of each variable. The parameters of those distributions can be predicted based on wave characteristics, the structure crest freeboard and the water depth at the toe of the breakwater, as shown in Eqs. (4), (6), (8), (10), and (12). A satisfactory performance of the proposed distributions is obtained for the three variables with $0.67 \leq R^2 \leq 0.78$ (see Figs. 13, 24 and 25).

The bivariate dependence between the variables is described through bivariate copulas. Gaussian, Clayton and Gumbel copulas are recommended for the pairs h_c/H_{m0} and $u_c/\sqrt{gH_{m0}}$, h_s/H_{m0} and V/H_{m0}^2 and V/H_{m0}^2 and $u_c/\sqrt{gH_{m0}}$, respectively. Eq. (20) is recommended to estimate the parameter of the Gaussian copula, which only depends on h_s/H_{m0}. Constant values of $\delta_{hV} = 0.8$ and $\theta_{Vu} = 1.2$ are recommended for Clayton and Gumbel copulas, respectively. A satisfactory prediction of the joint non-exceedance probabilities or the three variables is obtained with $0.97 \leq R^2 \leq 0.98$ (see Figs. 15, 31 and 32).

Finally, the use of the proposed model is illustrated to estimate the probability of fulfilling at least one tolerability limit of the three variables (OR probability). This is, the proposed model allows for the computation of the probability of functional failure of a mound breakwater due to overtopping. A one-tree vine-copula model is recommended using the Clayton and Gumbel copulas for the pairs h_s/H_{m0} and V/H_{m0}^2 and V/H_{m0}^2 and $u_c/\sqrt{gH_{m0}}$, respectively.

The OR probability is computed both considering the dependence and assuming independence between the variables and a significant difference is obtained. Therefore, it can be concluded that by accounting for the multivariate dependence between the variables, it is possible to reduce the crest freeboard and, thus, the material consumption. Thus, the use of the proposed model allows for a more economic design within the required safety level.

The expressions proposed in this study are valid within the experimental ranges that are given together with each derived equation. Therefore, checking their validity out of the experimental ranges of this study is encouraged, also considering the possible influence of crest walls, berms, and different armor layers and slopes. Moreover, since this study is motivated by climate change adaptation to overtopping hazard, a study where the methodology is used to account for possible climate scenarios is recommended.

Table 6
Number of tests where each marginal distribution function provided the best fit for those tests performed with a double-layer randomly-placed cube-armored model.

Distr.	Gamma	Logn.	Norm.	Expon.	GEV	Rayl.
h_c/H_{m0}	**21**	**22**	12	0	7	0
$u_c/\sqrt{gH_{m0}}$	15	**33**	6	0	8	0
V/H_{m0}^2	6	**31**	0	16	7	2

Table 7
Number of tests where each marginal distribution function provided the best fit for those tests performed with a single-layer Cubipod®-armored model.

Distr.	Gamma	Logn.	Norm.	Expon.	GEV	Rayl.
h_c/H_{m0}	**21**	12	8	0	9	0
$u_c/\sqrt{gH_{m0}}$	13	**24**	2	0	8	0
V/H_{m0}^2	11	**17**	0	14	3	2

Table 8
Number of tests where each marginal distribution function provided the best fit for those tests performed with a double-layer randomly-placed rock-armored model.

Distr.	Gamma	Logn.	Norm.	Expon.	GEV	Rayl.
h_c/H_{m0}	**3**	2	**3**	0	1	0
$u_c/\sqrt{gH_{m0}}$	0	**8**	0	0	1	0
V/H_{m0}^2	0	**2**	0	1	5	1

CRediT authorship contribution statement

Patricia Mares-Nasarre: Writing – original draft, Software, Methodology, Formal analysis, Conceptualization. **Marcel R.A. van Gent:** Writing – review & editing. **Oswaldo Morales-Nápoles:** Writing – review & editing, Methodology.

Declaration of competing interest

The authors declare that they have no known competing financial interests or personal relationships that could have appeared to influence the work reported in this paper.

Data availability

Data will be made available on request.

Acknowledgment

The authors want to acknowledge Prof. Dr. Josep R. Medina Folgado for providing the experimental data.

Appendix A. Marginal distributions

A.1. Marginal selection by armor element

In this section, the number of tests where each distribution function provided the best fit per armor layer is displayed in Tables 6–8. No relevant differences can be observed between the different armor layers.

A.2. Influence of explanatory variables in the parameters of the marginal distributions

Figs. 17 and 18 present the influence of the explanatory variables in Section 2.4 on the parameters of the Lognormal distribution to model h_c/H_{m0}.

Fig. 19 presents the Spearman's correlation coefficient (Spearman, 1904), r, calculated between the explanatory variables and the parameters μ_u or σ_u. r assesses the strength and direction of association between two ranked variables. This is, it provides a measure of monotonicity of the relation between two variables. $r \in [-1, 1]$, where $r = 1$ and -1 represent perfect positive and negative monotonic dependence, respectively. r is defined as

$$r = \frac{Cov[R(X), R(Y)]}{\sigma_{R(X)}\sigma_{R(Y)}} \tag{25}$$

where $Cov[R(X), R(Y)]$ is the covariance of the ranked variables, and $\sigma_{R(X)}$ and $\sigma_{R(Y)}$ are the standard deviations of the ranked variables.

As shown in Fig. 19, the correlation between the explanatory variables and the parameter μ_u is very low. In Fig. 20 the relationship between μ_u and the explanatory variables is presented as scatter plots.

In Fig. 21 the relationship between σ_u and the explanatory variables is displayed.

Figs. 22 and 23 show the influence of the explanatory variables in Section 2.4 on the parameters of the Lognormal distribution to model V/H_{m0}^2.

A.3. Goodness of fit of marginal distributions

Here, the comparison between the measured and estimated quantiles of h_c/H_{m0} and $u_c/\sqrt{gH_{m0}}$ using the developed formulas in Section 5 is displayed in Figs. 24 and 25.

Appendix B. Bivariate copulas

B.1. Rank correlation coefficients

In this section, the rank correlation between each pair of variables is studied. Fig. 26 presents the rank correlations between each pair of variables for each physical test. Fig. 27 presents the $p-values$ associated to those rank correlations. Note that $p - value < 0.05$ indicate that the measured rank correlation is significant.

B.2. Copulas

In this study, three copula families were used: Gaussian, Clayton and Gumbel. The Gaussian or normal copula is given by

$$C_\rho(u, v) = \Phi_\rho\{\Phi^{-1}(u), \Phi^{-1}(v)\} \tag{26}$$

where $\Phi_\rho\{.,.,.\}$ is the cumulative distribution function of the bivariate normal with 0 expectation, unit variance and ρ Pearson correlation coefficient (Pearson and Galton, 1895).

Clayton and Gumbel copulas are part of the Archimedean family of copulas. Clayton copula is parameterized by $\delta > 0$ and is given by

$$C_\delta(u, v) = (u^{-\delta} + u^{-\delta} - 1)^{-1/\delta} \tag{27}$$

Gumbel copula is parameterized by $\theta > 1$ and is given by

$$C_\theta(u, v) = exp[-([-ln(u)]^\theta + [-ln(u)]^\theta)^{1/\theta}] \tag{28}$$

B.3. Copula selection by armor element

In this section, the number of tests where each copula provided the best fit per armor layer is displayed in Tables 9–11. No relevant differences can be observed between the different armor layers.

B.4. Copula parameters and explanatory variables

Figs. 29 and 30 present the influence of the explanatory variables in Section 2.4 on the parameters of the Gaussian, Clayton and Gumbel copula to model the structure dependence between the pairs h_c/H_{m0} and $u_c/\sqrt{gH_{m0}}$, h_c/H_{m0} and V/H_{m0}^2 and V/H_{m0}^2 and $u_c/\sqrt{gH_{m0}}$, respectively.

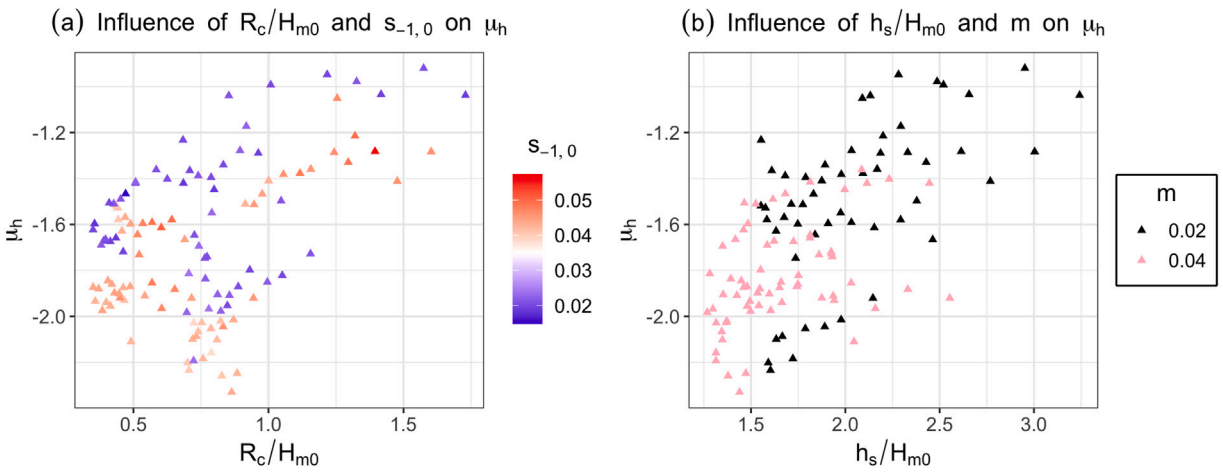

Fig. 17. Influence of explanatory variables on μ_h.

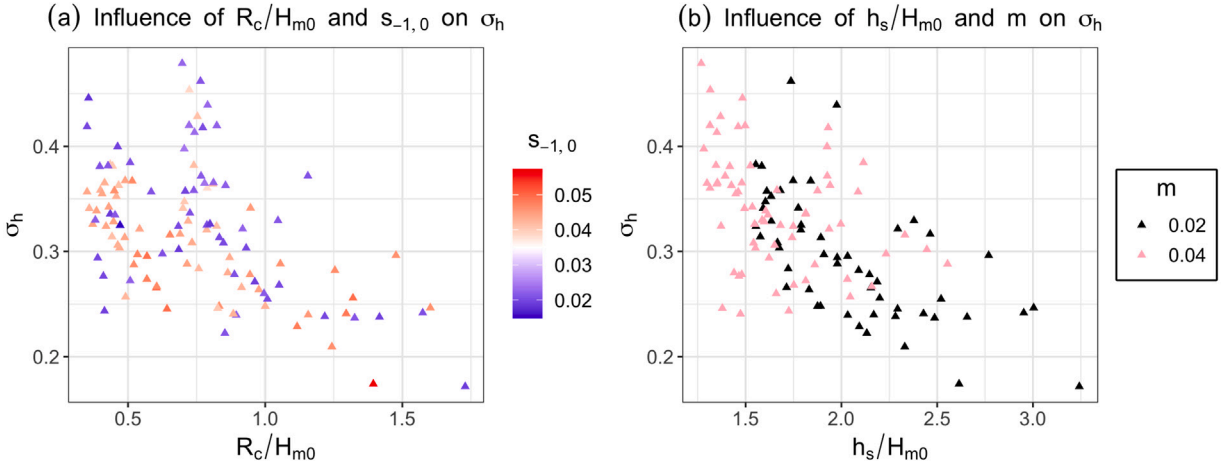

Fig. 18. Influence of explanatory variables on σ_h.

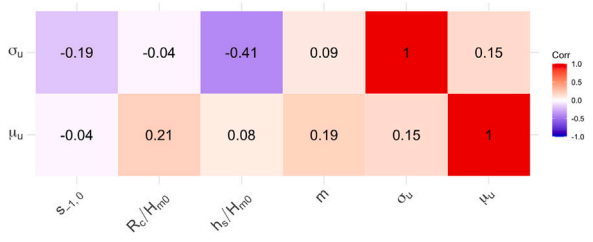

Fig. 19. Rank correlation matrix between explanatory variables and μ_u and σ_u.

Table 9
Best fit copulas for pairs with significant rank correlation for double-layer randomly-placed cube armor.

Copula	Gaussian	Frank	Clayton	Gumbel	Other
$h_c/H_{m0} - u_c/\sqrt{gH_{m0}}$	**4**	0	**4**	3	3
$h_c/H_{m0} - V/H_{m0}^2$	**12**	7	9	9	0
$V/H_{m0}^2 - u_c/\sqrt{gH_{m0}}$	0	3	4	**6**	0

Table 10
Best fit copulas for pairs with significant rank correlation for single-layer Cubipod® armor.

Copula	Gaussian	Frank	Clayton	Gumbel	Other
$h_c/H_{m0} - u_c/\sqrt{gH_{m0}}$	**3**	2	1	**3**	1
$h_c/H_{m0} - V/H_{m0}^2$	6	2	**13**	10	0
$V/H_{m0}^2 - u_c/\sqrt{gH_{m0}}$	0	1	**4**	**4**	0

Table 11
Best fit copulas for pairs with significant rank correlation for double-layer randomly-placed rock armor.

Copula	Gaussian	Frank	Clayton	Gumbel	Other
$h_c/H_{m0} - u_c/\sqrt{gH_{m0}}$	**1**	0	0	0	**1**
$h_c/H_{m0} - V/H_{m0}^2$	0	2	1	**3**	0
$V/H_{m0}^2 - u_c/\sqrt{gH_{m0}}$	0	0	0	**1**	0

B.5. Goodness of fit of copula models

Here, the comparison between the measured and estimated non-exceedance joint probabilities of the pairs h_c/H_{m0} and V/H_{m0}^2 and V/H_{m0}^2 and $u_c/\sqrt{gH_{m0}}$ is presented in Figs. 31 and 32, respectively.

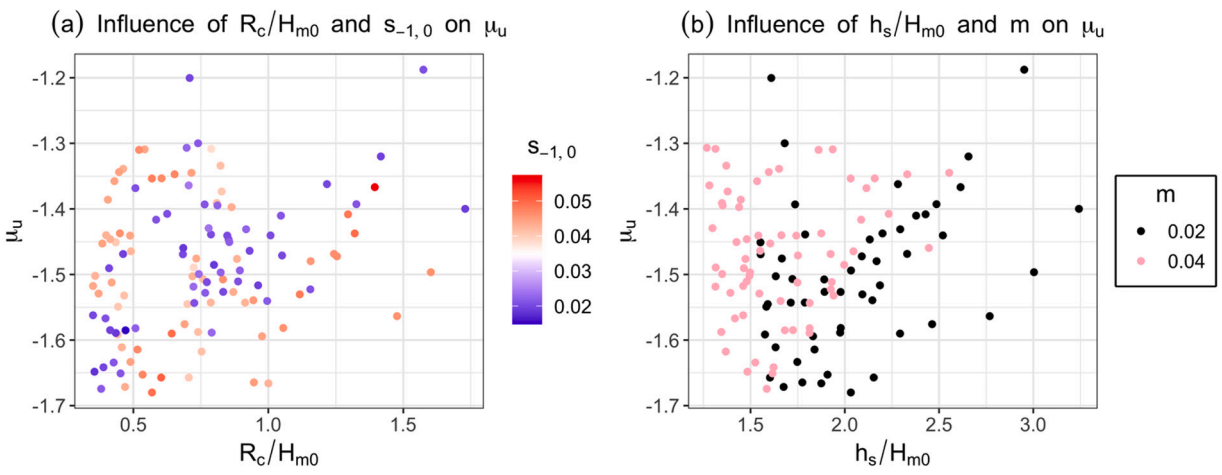

Fig. 20. Influence of explanatory variables on μ_u.

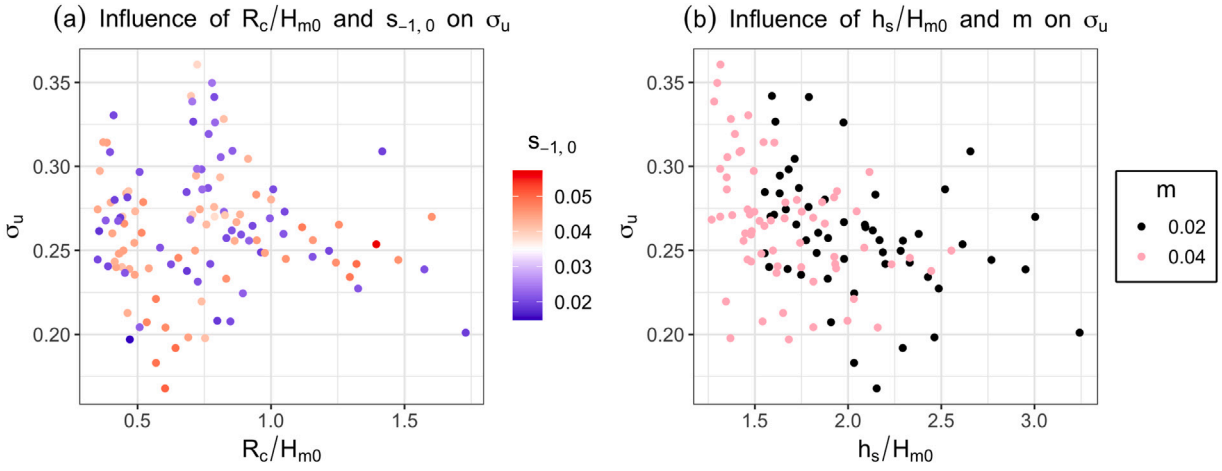

Fig. 21. Influence of explanatory variables on σ_u.

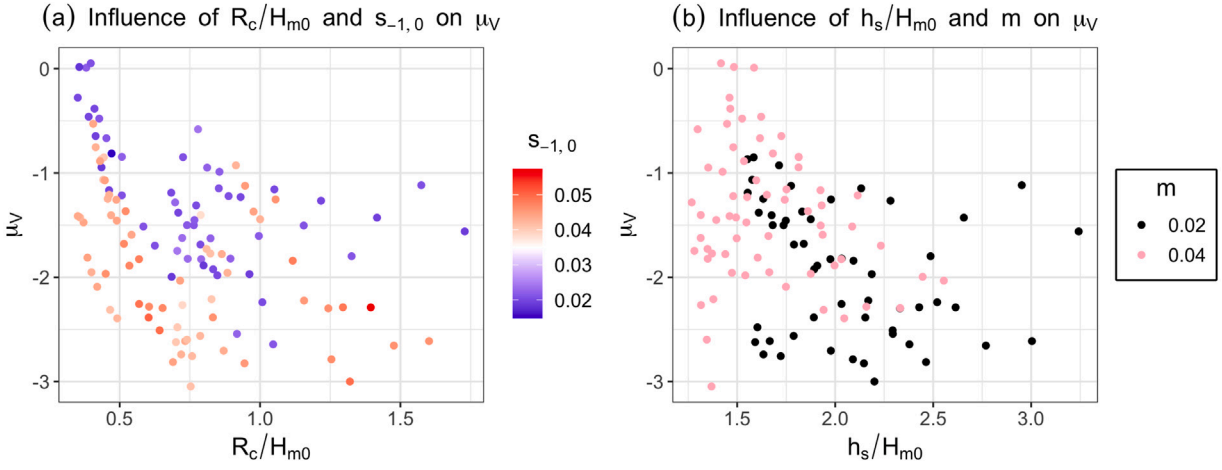

Fig. 22. Influence of explanatory variables on μ_V.

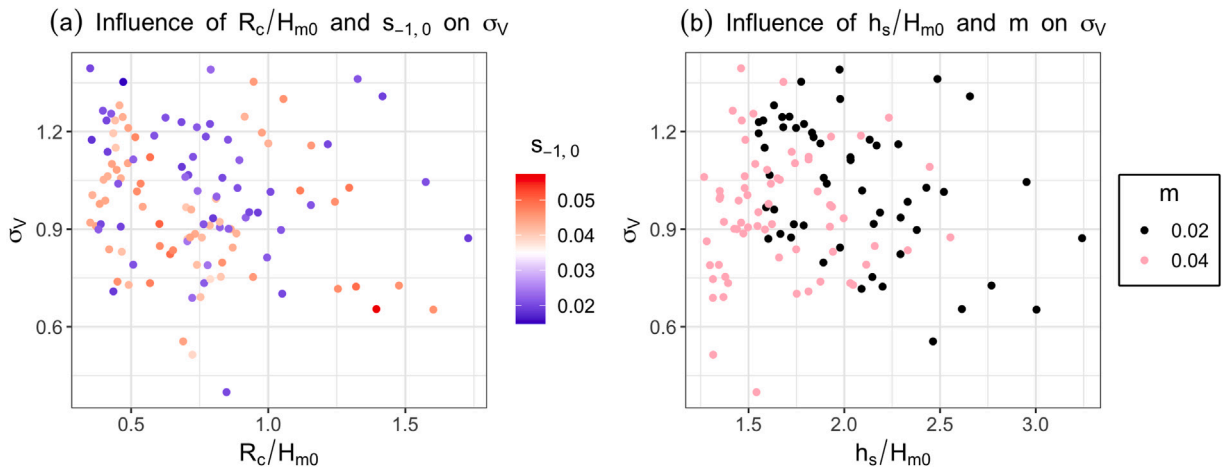

Fig. 23. Influence of explanatory variables on σ_V.

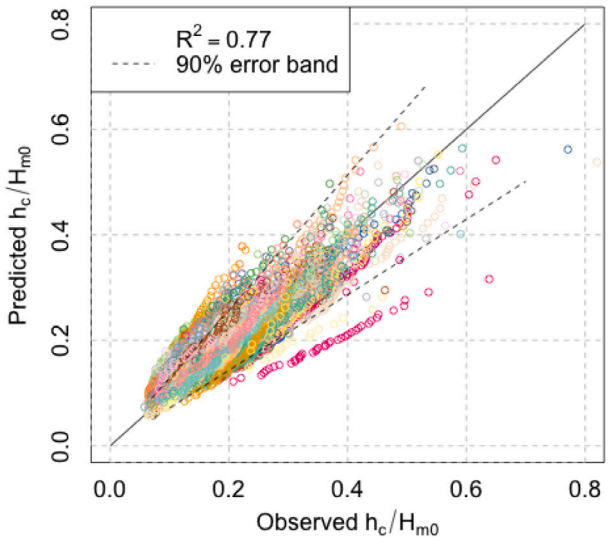

Fig. 24. Comparison between the measured and estimated h_c/H_{m0} marginal distributions with Lognormal distribution in Eq. (3) and parameters in Eq. (4) and (6).

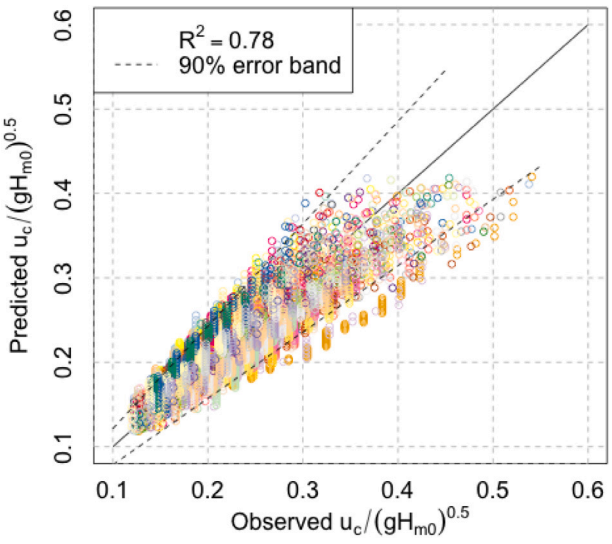

Fig. 25. Comparison between the measured and estimated $u_c/\sqrt{gH_{m0}}$ marginal distributions with Lognormal distribution in Eq. (3) and parameters $\mu_u = -1.5$ and (8).

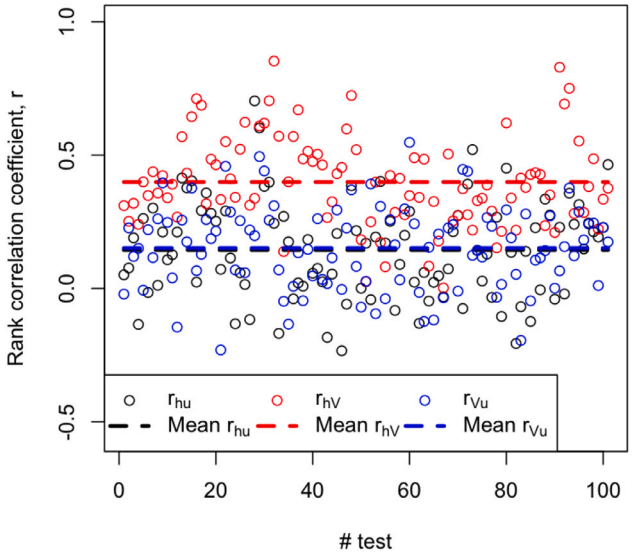

Fig. 26. Rank correlations for each test between h_c/H_{m0}, $u_c/\sqrt{gH_{m0}}$ and V/H_{m0}^2.

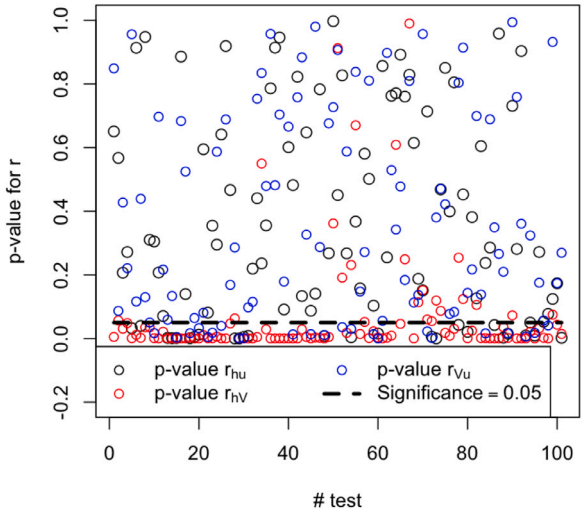

Fig. 27. P-values for rank correlation coefficients between h_c/H_{m0}, $u_c/\sqrt{gH_{m0}}$ and V/H_{m0}^2.

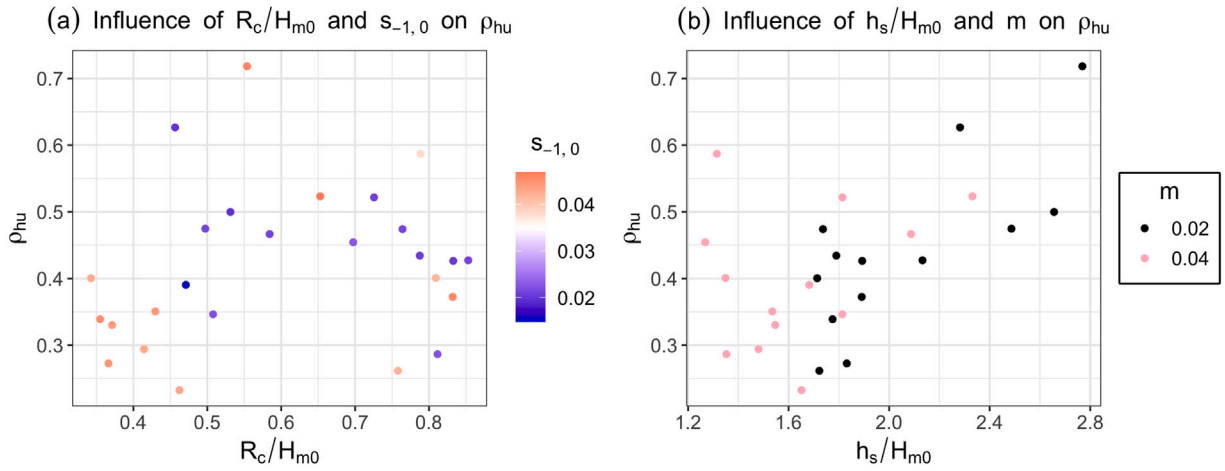

Fig. 28. Influence of explanatory variables on ρ_{hu}.

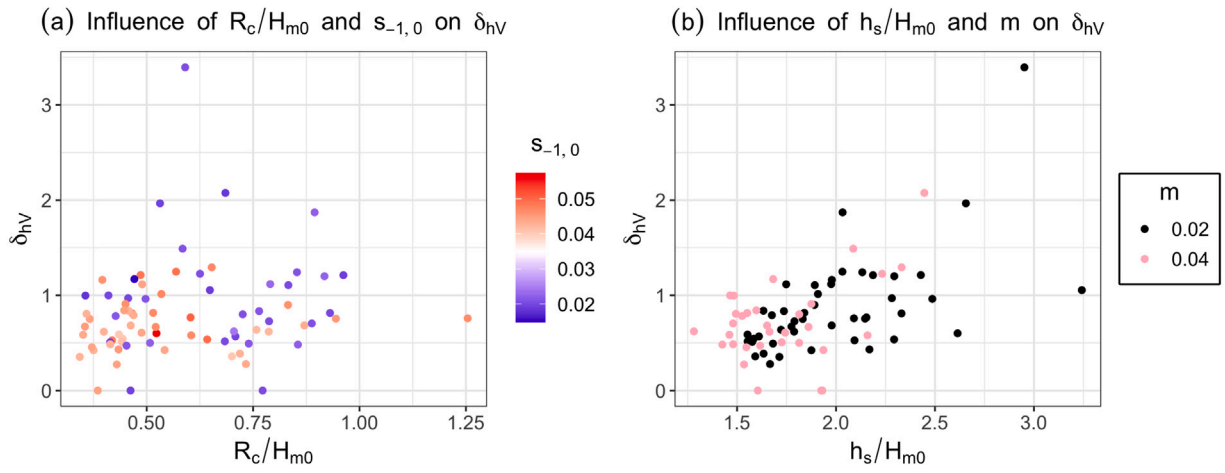

Fig. 29. Influence of explanatory variables on δ_{hV}.

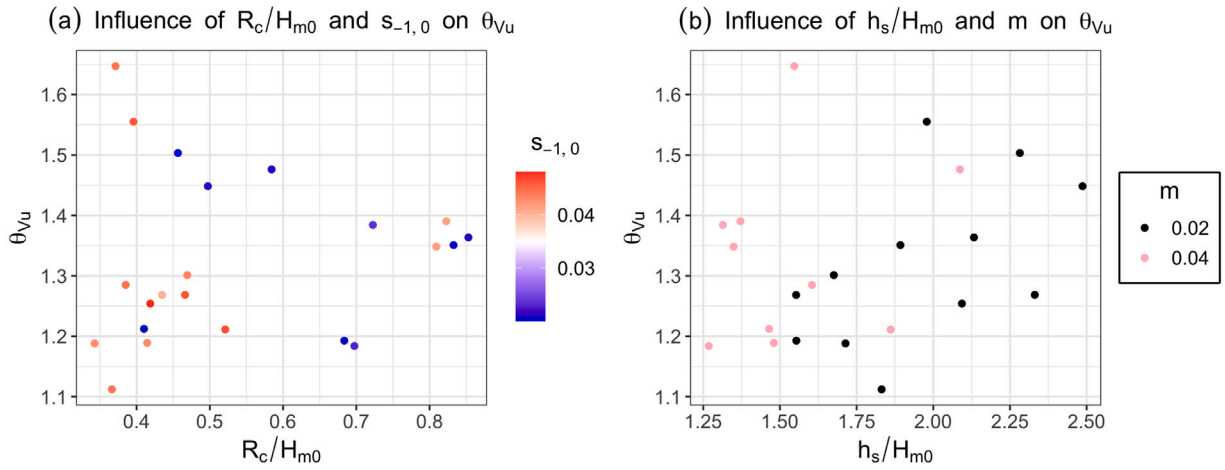

Fig. 30. Influence of explanatory variables on θ_{Vu}.

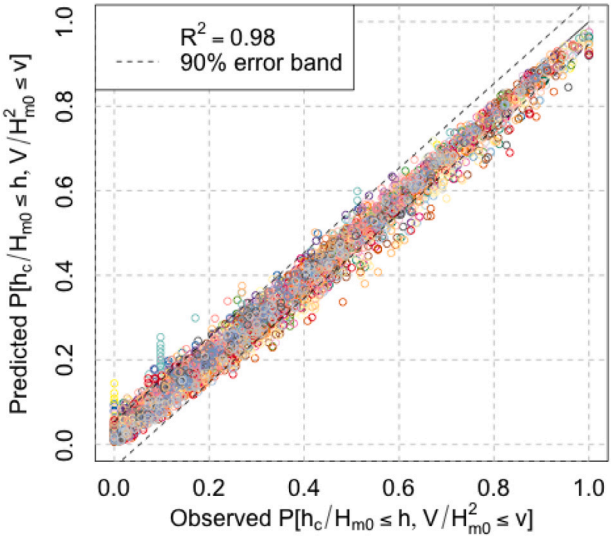

Fig. 31. Comparison between the observed and estimated non-exceedance joint probabilities for the pair $h_c/H_{m0} - V/H_{m0}^2$.

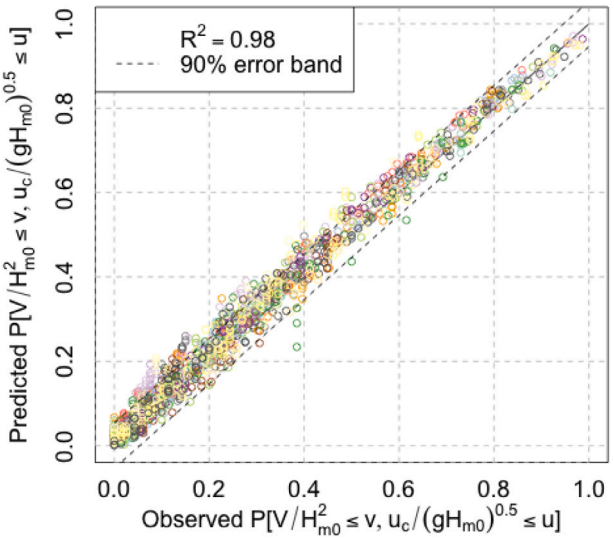

Fig. 32. Comparison between the observed and estimated non-exceedance joint probabilities for the pair $V/H_{m0}^2 - u_c/\sqrt{gH_{m0}}$.

References

Aas, K., Czado, C., Frigessi, A., Bakken, H., 2009. Pair-copula constructions of multiple dependence. Insurance Math. Econom. 44 (2), 182–198. http://dx.doi.org/10.1016/j.insmatheco.2007.02.001.

Akaike, H., 1973. Information Theory and an Extension of the Maxmum Likelihood Principale. Akademia Kiado, pp. 267–281.

Anderson, T.W., Darling, D.A., 1952. Asymptotic theory of certain "Goodness of Fit" criteria based on stochastic processes. Ann. Math. Stat. 23 (2), 193–212. http://dx.doi.org/10.1214/aoms/1177729437.

Anderson, T.W., Darling, D.A., 1954. A test of goodness of fit. J. Amer. Statist. Assoc. 49 (268), 765–769. http://dx.doi.org/10.2307/2281537.

Antão, E., Guedes Soares, C., 2014. Approximation of bivariate probability density of individual wave steepness and height with copulas. Coast. Eng. 89, 45–52. http://dx.doi.org/10.1016/j.coastaleng.2014.03.009.

Argente, G., Gómez-Martín, M.E., Medina, J.R., 2018. Hydraulic stability of the armor layer of overtopped breakwaters. J. Mar. Sci. Eng. 6 (4), http://dx.doi.org/10.3390/jmse6040143.

Bae, H., Yun, K., Yoon, J., Lim, N., 2016. Human stability with respect to overtopping flow on the breakwater. Int. J. Appl. Eng. Res. 11, 111–119.

Battjes, J.A., Groenendijk, H.W., 2000. Wave height distributions on shallow foreshores. Coast. Eng. 40 (3), 161–182. http://dx.doi.org/10.1016/S0378-3839(00)00007-7.

Besley, P., 1999. Overtopping of Sea-Walls-Design and Assessment Manual. R & D Technical Report. Tech. Rep., Vol. 178, Environment Agency, Bristol, UK.

Bruce, T., Van der Meer, J., Franco, L., Pearson, J.M., 2009. Overtopping performance of different armour units for rubble mound breakwaters. Coast. Eng. 56 (2), 166–179. http://dx.doi.org/10.1016/j.coastaleng.2008.03.015.

Camus, P., Tomás, A., Díaz-Hernández, G., Rodríguez, B., Izaguirre, C., Losada, I., 2019. Probabilistic assessment of port operation downtimes under climate change. Coast. Eng. 147, 12–24. http://dx.doi.org/10.1016/j.coastaleng.2019.01.007.

Corbella, S., Stretch, D.D., 2013. Simulating a multivariate sea storm using archimedean copulas. Coast. Eng. 76, 68–78. http://dx.doi.org/10.1016/j.coastaleng.2013.01.011.

Czado, C., 2019. Analyzing Dependent Data with Vine Copulas. In: Lecture Notes in Statistics, Vol. 222, Springer, http://dx.doi.org/10.1007/978-3-030-13785-4_1.

De Michele, C., Salvadori, G., Passoni, G., Vezzoli, R., 2007. A multivariate model of sea storms using copulas. Coast. Eng. 54 (10), 734–751. http://dx.doi.org/10.1016/j.coastaleng.2007.05.007.

de Ridder, M.P., Kramer, J., den Bieman, J.P., Wenneker, I., 2023. Validation and practical application of nonlinear wave decomposition methods for irregular waves. Coast. Eng. 183, 104311. http://dx.doi.org/10.1016/j.coastaleng.2023.104311.

EurOtop, 2018. Manual on Wave Overtopping of Sea Defences and Related Structures. an Overtopping Manual Largely Based on European Research, But for Worldwide Application.. URL www.overtopping-manual.com.

Figueres, M., Medina, J.R., 2005. Estimating incident and reflected waves using a fully nonlinear wave model. In: Coastal Engineering 2004: (in 4 Volumes). World Scientific, pp. 594–603.

Franco, L., De Gerloni, M., Van der Meer, J., 1994. Wave overtopping on vertical and composite breakwaters. In: Proc. ICCE 1994. pp. 1030–1045.

Geeraerts, J., Troch, P., De Rouck, J., Verhaeghe, H., Bouma, J.J., 2007. Wave overtopping at coastal structures: prediction tools and related hazard analysis. J. Clean. Prod. 15 (16), 1514–1521. http://dx.doi.org/10.1016/j.jclepro.2006.07.050.

Genest, C., Quessy, J.-F., Rémillarf, B., 2006. Goodness-of-fit procedures for copula models based on the probability integral transformation. Scand. J. Stat. 33 (2), 337–366. http://dx.doi.org/10.1111/j.1467-9469.2006.00470.x.

Genest, C., Rémillard, B., Beaudoin, D., 2009. Goodness-of-fit tests for copulas: A review and a power study. Insurance Math. Econom. 44 (2), 199–213. http://dx.doi.org/10.1016/j.insmatheco.2007.10.005.

Herrera, M.P., Medina, J.R., 2015. Toe berm design for very shallow waters on steep sea bottoms. Coast. Eng. 103, 67–77. http://dx.doi.org/10.1016/j.coastaleng.2015.06.005.

IPCC, 2019. Special Report on the Ocean and Cryosphere in a Changing Climate. Chapter 4: Sea Level Rise and Implications for Low-Lying Islands, Coasts and Communities.. Tech. Rep., https://www.ipcc.ch/site/assets/uploads/sites/3/2019/11/08_SROCC_Ch04_FINAL.pdf Accessed: 15th june 2020.

Jaeger, W.S., Morales-Nápoles, O., 2017. A vine-copula model for time series of significant wave heights and mean zero-crossing periods in the north sea. ASCE-ASME J. Risk Uncertain. Eng. Syst. A 3, 04017014.

Joe, H., 1997. Multivariate Models and Multivariate Dependence Concepts. CRC Press, http://dx.doi.org/10.1201/9780367803896.

Joe, H., 2014. Dependence Modeling with Copulas (1St Ed.). Chapman and Hall/CRC, http://dx.doi.org/10.1201/b17116.

Kolmogorov, A.N., 1933. Sulla determinazione empirica di una legge didistribuzione. Giorn Dell'inst Ital Degli Att 4, 89–91.

Koosheh, A., Etemad-Shahidi, A., Cartwright, N., Tomlinson, R., van Gent, M.R.A., 2021. Individual wave overtopping at coastal structures: A critical review and the existing challenges. Appl. Ocean Res. 106, 102476. http://dx.doi.org/10.1016/j.apor.2020.102476.

Koosheh, A., Etemad-Shahidi, A., Cartwright, N., Tomlinson, R., van Gent, M.R., 2022. Distribution of individual wave overtopping volumes at rubble mound seawalls. Coast. Eng. 177, 104173. http://dx.doi.org/10.1016/j.coastaleng.2022.104173.

Leontaris, G., Morales-Nápoles, O., Wolfert, A., 2016. Probabilistic scheduling of offshore operations using copula based environmental time series – An application for cable installation management for offshore wind farms. Ocean Eng. 125, 328–341. http://dx.doi.org/10.1016/j.oceaneng.2016.08.029.

Lira-Loarca, A., Cobos, M., Losada, M.Á., Baquerizo, A., 2020. Storm characterization and simulation for damage evolution models of maritime structures. Coast. Eng. 156, 103620. http://dx.doi.org/10.1016/j.coastaleng.2019.103620.

Lucio, D., Tomás, A., Lara, J., Camus, P., Losada, I., 2020. Stochastic modeling of long-term wave climate based on weather patterns for coastal structures applications. Coast. Eng. 161, 103771. http://dx.doi.org/10.1016/j.coastaleng.2020.103771.

Mansard, E.P.D., Funke, E.R., 1980. The measurement of incident and reflected spectra using a least squares method. In: Coastal Engineering 1980. pp. 154–172.

Mares-Nasarre, P., Argente, G., Gómez-Martín, M.E., Medina, J.R., 2019. Overtopping layer thickness and overtopping flow velocity on mound breakwaters. Coast. Eng. 154, 103561. http://dx.doi.org/10.1016/j.coastaleng.2019.103561.

Mares-Nasarre, P., Gómez-Martín, M.E., Medina, J.R., 2020a. Influence of mild bottom slopes on the overtopping flow over mound breakwaters under depth-limited breaking wave conditions. J. Mar. Sci. Eng. 8 (1), 3. http://dx.doi.org/10.3390/jmse8010003.

Mares-Nasarre, P., Molines, J., Gómez-Martín, M.E., Medina, J.R., 2020b. Individual wave overtopping volumes on mound breakwaters in breaking wave conditions and gentle sea bottoms. Coast. Eng. 159, 103703. http://dx.doi.org/10.1016/j.coastaleng.2020.103703.

Mares-Nasarre, P., Molines, J., Gómez-Martín, M.E., Medina, J.R., 2021. Explicit neural network-derived formula for overtopping flow on mound breakwaters in depth-limited breaking wave conditions. Coast. Eng. 164, 103810. http://dx.doi.org/10.1016/j.coastaleng.2020.103810.

Masina, M., Lamberti, A., Archetti, R., 2015. Coastal flooding: A copula based approach for estimating the joint probability of water levels and waves. Coast. Eng. 97, 37–52. http://dx.doi.org/10.1016/j.coastaleng.2014.12.010.

Molines, J., Herrera, M.P., Gómez-Martín, M.E., Medina, J.R., 2019. Distribution of individual wave overtopping volumes on mound breakwaters. Coast. Eng. 149, 15–27. http://dx.doi.org/10.1016/j.coastaleng.2019.03.006.

Molines, J., Medina, J.R., 2016. Explicit wave-overtopping formula for mound breakwaters with crown walls using CLASH neural network–derived data. J. Waterw. Port Coast. Ocean Eng. 142 (3), 04015024. http://dx.doi.org/10.1061/(ASCE)WW.1943-5460.0000322.

Nagler, T., Schepsmeier, U., Stoeber, J., Brechmann, E.C., Graeler, B., Erhardt, T., Almeida, C., Min, A., Czado, C., Hofmann, M., 2022. VineCopula: Statistical inference of vine copulas. URL https://cran.r-project.org/package=VineCopula R package version 2.4.4.

Nelsen, R.B., 2006. An Introduction To Copulas (Springer Series in Statistics). Springer-Verlag, Berlin, Heidelberg, http://dx.doi.org/10.5555/1204326.

Nørgaard, J.Q.H., Andersen, T.L., Burcharth, H.F., 2014. Distribution of individual wave overtopping volumes in shallow water wave conditions. Coast. Eng. 83, 15–23. http://dx.doi.org/10.1016/j.coastaleng.2013.09.003.

Pearson, K., Galton, F., 1895. VII. Note on regression and inheritance in the case of two parents. Proc. R. Soc. Lond. 58 (347–352), 240–242. http://dx.doi.org/10.1098/rspl.1895.0041.

Romano, A., Bellotti, G., Briganti, R., Franco, L., 2015. Uncertainties in the physical modelling of the wave overtopping over a rubble mound breakwater: The role of the seeding number and of the test duration. Coast. Eng. 103, 15–21. http://dx.doi.org/10.1016/j.coastaleng.2015.05.005.

Salvadori, G., Durante, F., Tomasicchio, G., D'Alessandro, F., 2015. Practical guidelines for the multivariate assessment of the structural risk in coastal and off-shore engineering. Coast. Eng. 95, 77–83. http://dx.doi.org/10.1016/j.coastaleng.2014.09.007.

Salvadori, G., Michele, C.D., Kottegoda, N.T., Rosso, R., 2007. Extremes in Nature. An Approach Using Copulas. Sprinter, http://dx.doi.org/10.1007/1-4020-4415-1.

Salvadori, G., Tomasicchio, G., D'Alessandro, F., 2014. Practical guidelines for multivariate analysis and design in coastal and off-shore engineering. Coast. Eng. 88, 1–14. http://dx.doi.org/10.1016/j.coastaleng.2014.01.011.

Schüttrumpf, H., van Gent, M.R.A., 2004. Wave overtopping at seadikes. In: Coastal Structures 2003. pp. 431–443. http://dx.doi.org/10.1061/40733(147)36.

Sebastian, A., Dupuits, E., Morales-Nápoles, O., 2017. Applying a Bayesian network based on Gaussian copulas to model the hydraulic boundary conditions for hurricane flood risk analysis in a coastal watershed. Coast. Eng. 125, 42–50. http://dx.doi.org/10.1016/j.coastaleng.2017.03.008.

Sibuya, M., et al., 1960. Bivariate extreme statistics. Ann. Inst. Statist. Math. 11 (2), 195–210. http://dx.doi.org/10.1007/BF01682329.

Sklar, M., 1959. Fonctions de repartition a n dimensions et leurs marges. Publ. Inst. Stat. Univ. Paris 8, 229–231, URL https://cir.nii.ac.jp/crid/1573387449735953792.

Smirnov, N., 1948. Table for estimating the goodness of fit of empirical distributions. Ann. Math. Stat. 19 (2), 279–281.

Spearman, C., 1904. The proof and measurement of association between two things. Am. J. Psychol. 15 (1), 72–101.

Torres-Alves, G.A., Morales-Nápoles, O., 2020. Reliability analysis of flood defenses: The case of the nezahualcoyotl dike in the aztec city of tenochtitlan. Reliab. Eng. Syst. Saf. 203, 107057. http://dx.doi.org/10.1016/j.ress.2020.107057.

van Gent, M.R.A., 1999. Physical Model Investigations on Coastal Structures with Shallow Foreshores: 2D Model Tests with Single and Double-Peaked Wave Energy Spectra. Tech. Rep..

van Gent, M.R.A., 2003. Wave overtopping events at dikes. In: Proc. ICCE 2002, Cardiff. Vol. 2. World Scientific, pp. 2203–2215. http://dx.doi.org/10.1142/9789812791306_0185.

van Gent, M.R.A., Wolters, G., Capel, A., 2022. Wave overtopping discharges at rubble mound breakwaters including effects of a crest wall and a berm. Coast. Eng. 176, 104151. http://dx.doi.org/10.1016/j.coastaleng.2022.104151.

Verhagen, H.J., van Vledder, G., Arab, S.E., 2009. A practical method for design of coastal structures in shallow water. In: Coastal Engineering 2008: (in 5 Volumes). World Scientific, pp. 2912–2922.

WCED, 1987. Our Common Future. World Commission on Environment and Development.. URL https://digitallibrary.un.org/record/139811.

Zanuttigh, B., van der Meer, J., Bruce, T., Hughes, S., 2013. Statistical characterisation of extreme overtopping wave volumes. In: Proc. Coasts, Marine Structures and Breakwaters. 2014. Vol. 1, ICE Publishing, London, UK, pp. 442–451.

Zhang, Y., Kim, C.-W., Beer, M., Dai, H., Soares, C.G., 2018. Modeling multivariate ocean data using asymmetric copulas. Coast. Eng. 135, 91–111. http://dx.doi.org/10.1016/j.coastaleng.2018.01.008.